（1）大規模化合物ライブラリを使った化合物探索

今回化合物探索により購入した 103 化合物は、先行研究により得られている NACME 誘導体とは骨格が大きく異なるものである。従って、実験により酵素活性阻害効果が観察されれば新規骨格を有する阻害剤候補となり、阻害剤開発の成功率も向上すると期待している。

（2）NACME 誘導体の構造・物性と実験による酵素活性阻害のデータからの構造活性相関

今回得た統計モデルについては NACME 誘導体の化合物最適化研究に応用するため更なる検証・修正が必要であると思われる。これらの手法単独での使用ではなく、他の計算手法との組み合わせにより化合物設計の作業を効率化が可能であると期待している。

（3）量子化学的手法を用いた RT 内在の RNase H ドメインと薬剤複合体構構造のモデリング

QM/MM 法によりエネルギー極小化計算終了後、その電子状態を考慮されたポケット構造の観察が可能となる。これらの情報は RNase H のような特徴的なポケット構造を理解するには極めて有効となる。今後は、この構造情報を基盤にして、de novo design の技法、ドッキング研究、QM/MM 法による化合物最適化研究、（2）の構造活性相関の研究を組み合わせて応用したいと考えている。

E. 結論

本年度の研究により、今後行う化合物最適化計算の為の基本的情報（精密構造の入手、先行研究からの構造活性相関）が得られたと考えている。今後は、これらのデータを生かして新たな分子設計技法を構築できると確信している。

F. 研究危険情報

無し

G. 研究発表

（1） 論文発表

1. ○ Harada M, Murakami H, Okawa A, Okimoto N, Hiraoka S, Nakahara T, Akasaka R, Shiraishi Y, Futatsugi N, Mizutani-Koseki Y, Kuroiwa A, Shirouzu M, Yokoyama S, Taiji M, Iseki S, Ornitz DM, and Koseki H. FGF9 monomer-dimer equilibrium regulates extracellular matrix affinity and tissue diffusion. Nat Genet. 2009; 41(3): 289-298.
2. ○ Okimoto N, Futatsugi N, Fuji H, Suenaga A, Morimoto G, Yanai R, Ohno Y, Narumi T, and Taiji M.. High-performance drug discovery: computational screening by combining docking and molecular dynamics simulations. PLoS Comput Biol. 2009 Oct;5(10):e1000528.

（2） 学会発表

1. 沖本 憲明”タンパク質-リガンド結合親和性予測法の評価” SCHRODINGER ユーザーフォーラム, 2009 平成 21 年 10 月 21 日, 東京
2. 沖本 憲明” High-performance drug discovery: computational screening by combining docking and molecular dynamics simulations.”, the 54th Biophysical Society Annual Meeting, 平成 22 年 2 月 23, San Francisco
3. 沖本 憲明 “分子ドッキングと分子動力学計算を組み合わせた化合物スクリーニング” 日本薬学会 第 130 年会, 平成 22 年 3 月 29 日, 岡山

H. 知的財産権の出願・登録状況

（1）特許取得

無し

（2）実用新案登録

無し

（3）その他

無し

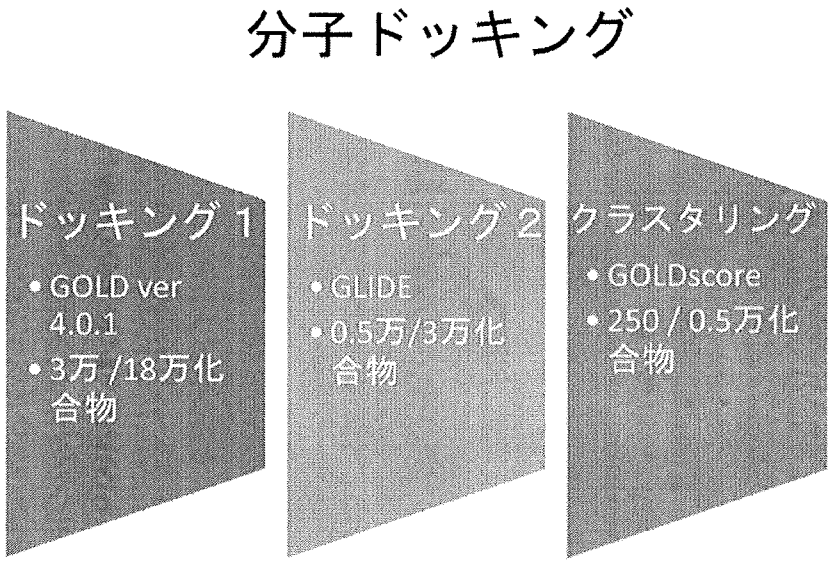

図１：分子ドッキング手順

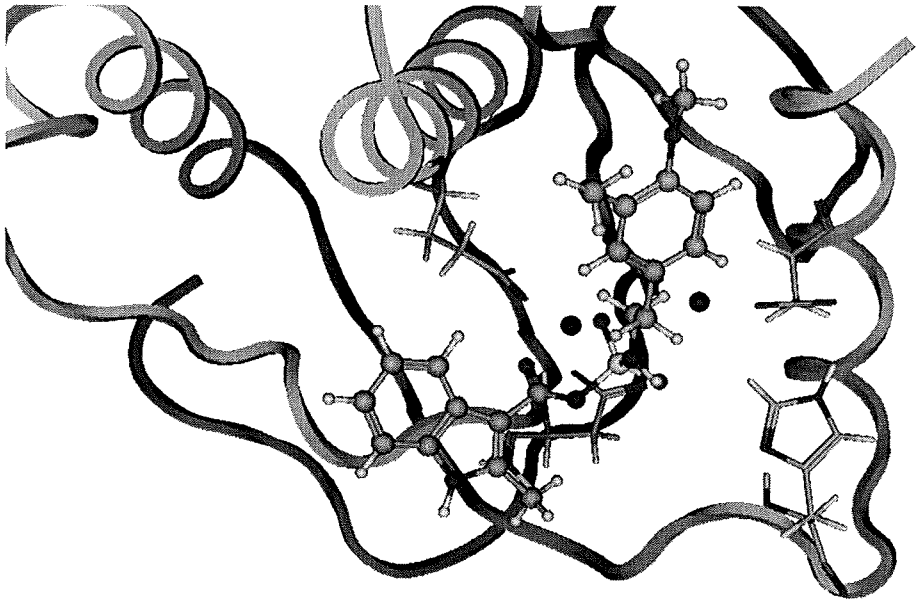

図２：ドッキングスコアが高かった化合物とタンパク質の相互作用

研究成果の刊行に関する一覧表

雑誌

発表者氏名	論文タイトル	発表誌名	巻号	ページ	出版年
Matsuyama S., Aydan A., Ode H., Hata M., Sugiura W., Hoshino T.	Structural and Energetic Analysis on the Complexes of Clinically-isolated Subtype C HIV-1 Proteases and Approved Inhibitors by Molecular Dynamics Simulation	J. Phys. Chem. B	114 (1)	521-530	2010
Urano E, Ichikawa R, Morikawa Y, Yoshida T, Koyanagi T, Komano J.	T cell-based functional cDNA library screening identified SEC14-like 1a carboxy-terminal domain as a negative regulator of human immunodeficiency virus replication	Vaccine		(in press)	2010
Kariya Y, Hamatake M, Urano E, Yoshiyama H, Shimizu N, Komano J.	A dominant-negative derivative of EBNA1 represses EBNA1-mediated transforming gene expression during the acute phase of Epstein-Barr virus infection independent of rapid loss of viral genome	Cancer Sci.		(in press)	2010
Hassan R, Suzu S, Hiyoshi M, Takahashi-Makise N, Ueno T, Agatsuma T, Akari H, Komano J, Takebe Y, Motoyoshi K and Okada S.	Dys-regulated activation of a Src tyroine kinase Hck at the Golgi disturbs *N*-glycosylation of a cytokine receptor Fms	J. Cell Physiol.	221(2)	458-468	2009
Iwatani Y., Chan D. S. B., Liu L., Yoshii H., Shibata J., Yamamoto N., Levin J. G., Gronenborn A. M., and Sugiura W.	HIV-1 Vif-mediated ubiquitination/degradation of APOBEC3G involves four critical lysine residues in its C-terminal domain	Proc. Natl. Acad. Sci. USA	106	19539-19544	2009
Iwatani Y.	Study on molecular mechanism of host defense factor, APOBEC3G, against HIV	J. AIDS Research	11	218-222	2009

Murakami T, Kumakura S, Yamazaki T, Tanaka R, Hamatake M, Okuma K, Huang W, Toma J, Komano J, Yanaka M, Tanaka Y, Yamamoto N.	The Novel CXCR4 Antagonist, KRH-3955 Is an Orally Bioavailable and Extremely Potent Inhibitor of Human Immunodeficiency Virus Type 1 Infection: Comparative Studies with AMD3100	Antimicro. Agents. Chemother.	53 (7)	2940-2948	2009
Iwasaki, Y., H. Akari, T. Murakami, S. Kumakura, Z. Dewan, M. Yanaka, and N. Yamamoto.	Efficient inhibition of SDF-1a-mediated chemotaxis and HIV-1 infection by novel CXCR4 antagonists.	Cancer Sci.	100	778-781	2009
村上　努	HIV 複製を制御する宿主因子の探索	The Journal of AIDS Research	11 (3)	205-209	2009
村上　努	HIV の粒子形成のメカニズム—Gag 蛋白に関する最新の知見—	Confronting HIV2009	35	5-7	2009
Harada M, Murakami H, Okawa A, Okimoto N, Hiraoka S, Nakahara T, Akasaka R, Shiraishi Y, Futatsugi N, Mizutani-Koseki Y, Kuroiwa A, Shirouzu M, Yokoyama S, Taiji M, Iseki S, Ornitz DM, and Koseki H	FGF9 monomer-dimer equilibrium regulates extracellular matrix affinity and tissue diffusion	Nat Genet.	41(3)	289-298	2009
Okimoto N, Futatsugi N, Fuji H, Suenaga A, Morimoto G, Yanai R, Ohno Y, Narumi T, and Taiji M.	High-performance drug discovery: computational screening by combining docking and molecular dynamics simulations	PLoS Comput. Biol.	5(10)	e1000528	2009

Structural and Energetic Analysis on the Complexes of Clinically Isolated Subtype C HIV-1 Proteases and Approved Inhibitors by Molecular Dynamics Simulation

Shou Matsuyama,[†] Ay Aydan,[†] Hirotaka Ode,[†] Masayuki Hata,[‡] Wataru Sugiura,[§,||] and Tyuji Hoshino*,[†]

Graduate School of Pharmaceutical Sciences, Chiba University, 1-33 Yayoi-cho, Inage-ku, Chiba 263-8522, Japan, College of Pharmaceutical Sciences, Matsuyama University, 4-2 Bunkyo-cho, Matsuyama 790-8578, Japan, AIDS Research Center, National Institute of Infectious Diseases, 4-7-1 Gakuen, Musashimurayama, Tokyo 208-1011, Japan, and Clinical Research Center, Nagoya Medical Center, 4-1-1 Sannomaru, naka-ku, Nagoya 460-0001, Japan

Received: August 28, 2009; Revised Manuscript Received: October 14, 2009

HIV-1 has a large genetic diversity. Subtype B HIV-1 is commonly found in patients in developed countries. In contrast, an increasing number of patients are infected with the non-B subtype viruses, especially with subtype C HIV-1, in developing countries. It remains to be clarified how mutations or polymorphisms in non-B subtype HIV-1 influence the efficacy of the approved inhibitors. In this study, we have performed molecular dynamics simulations on clinically isolated subtype C HIV-1 proteases in complex with three kinds of approved inhibitors. From the structural and energetic viewpoints, we identified the polymorphisms influencing on the binding of the inhibitors. The effect of the V82I mutation on the association with chemicals and the reason for rare appearance of the D30N mutation in subtype C HIV-1 were discussed in terms of the change of geometry of the residues in HIV-1 protease.

Introduction

Total number of patients infected with human immunodeficiency virus (HIV) is supposed to be 3.3 million in the world in 2007 and HIV infectious disease is still one of the serious threats to human beings.[1] HIV is separated into two types, HIV-1 and HIV-2, and most of the patients in the world carry HIV-1. According to its high genetic diversity, HIV-1 is classified into three groups, M (Main), O (Outlier), and N (non-M/non-O). Viruses in group M are further divided into nine subtypes and several circulating recombinant forms (CRFs). Among nine subtypes, subtype B HIV-1 is major in developed countries in North America and Europe. In contrast, the viruses other than subtype B, so-called non-B subtype HIV-1, are mainly found among patients in developing countries in Africa and South East Asia. Over half of the patients are infected with subtype C HIV-1 in the world.

HIV-1 has a gene coding the viral enzyme called HIV-1 protease (HIV-1 PR).[2] Since the inhibition of the action of this enzyme leads no maturation of viral precursor and incomplete replication of the virus,[3] the inhibitors against HIV-1 PR have been prescribed in the chemotherapy for HIV-1 infectious disease.[4−12] All the PR inhibitors released so far were mainly developed against subtype B HIV-1 PR. HIV-1 PR has a formation of homodimer and each monomer consists of 99 amino residues (Figure 1A). Polymorphisms are frequently observed in HIV-1 PRs.[13] For example, the K20I mutation dominantly appears in the PRs of subtype G and CRF02_AG, M36I appears in PRs of subtypes A, C, D, F, G, CRF01_AE, and CRF02_AG, V82I appears in subtype G, and I93L appears in subtype C. These polymorphisms are closely related to the difference in mutational pathways leading to emergence of the drug resistant variants among subtypes. As some epidemiological studies suggested, the polymorphisms in PRs will change drug efficacy among different subtypes.[14−24] It is interesting to note that some mutations such as D30N, which is known for the primary mutation for drug resistance in subtype B PR, are rarely seen in non-B subtype PRs.[18,25,26] A study based on the clinical data with hundreds of the subtype C- and subtype B-infected patients clearly suggested that a difference was observed in frequency of the D30N mutation between subtypes C and B, while little difference was seen for the L90 M mutation.[25] Further, significant differences were found in the rates of appearance of M36I, L63P, A71 V, V77I, and I93L between subtypes C and B. Hence, the difference in polymorphism between subtypes should be seriously considered for planning the chemotherapeutic protocol for the nonsubtype B-infected patients. Accordingly, the accumulation of the knowledge on the susceptibility of inhibitors or the emergence rate of drug resistant mutations is required for non-B subtype HIV-1.

In this study, we have performed molecular dynamics (MD) simulation on the complexes of clinically isolated subtype C HIV-1 PRs and its inhibitors. Three kinds of HIV-1 PRs are examined; two of them were isolated from patients who have no experience on the treatment with PR inhibitors, and one was isolated from a patient who failed in the therapy with one of the PR inhibitors; nelfinavir (NFV), because of the appearance of drug resistant mutations (Figure 1B, and Figure S1 and Table S1 in Supporting Information). Three kinds of inhibitors: atazanavir (ATV), nelfinavir (NFV) and saquinavir (SQV), have been examined through the present computational study (Figure 1C).

Additional MD simulations have been performed on the complexes of the subtype B HIV-1 PR and the inhibitors

* To whom correspondence should be addressed. Tel: +81-43-290-2926. Fax: +81-43-290-2925. E-mail: hoshino@faculty.chiba-u.jp.
[†] Chiba University.
[‡] Matsuyama University.
[§] National Institute of Infectious Diseases.
[||] Nagoya Medical Center.

10.1021/jp908314f
Published on Web 11/06/2009

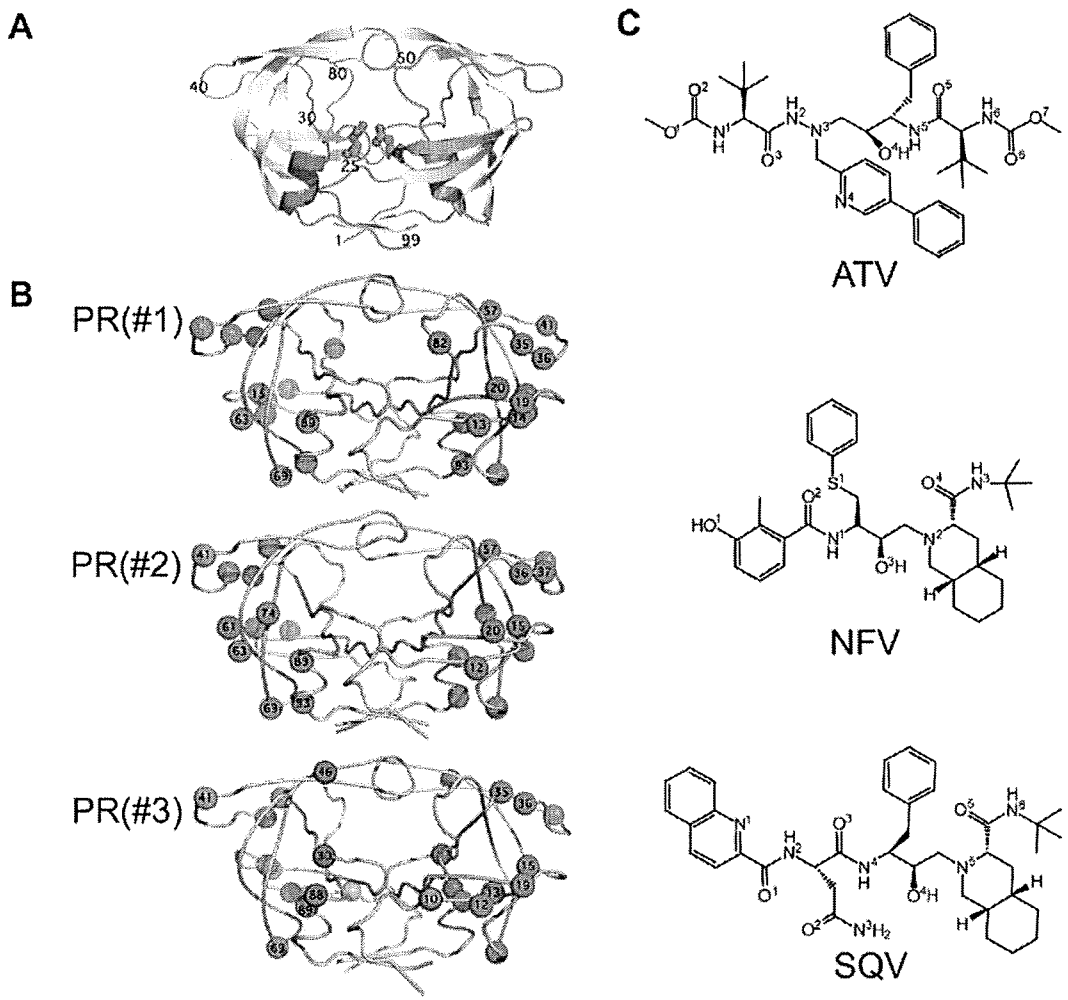

Figure 1. (A) Structure of HIV-1 PR. Locations of two catalytic aspartates are shown in the ball and stick representation. (B) Clinically isolated subtype C HIV-1 PR: PR(#1), PR(#2), and PR(#3). The red spheres indicate the D30N, M46L, and N88D mutations that are the primary mutations causing resistance to NFV. The orange sphere represents L10F, the secondary mutation to NFV. The green spheres represent the natural polymorphism seen in subtype C HIV-1 PR, differentiated from subtype B HIV-1 PR. The coloring of the spheres is based on HIVdb in Stanford University.[23] (C) Chemical structures of ATV, NFV, SQV.

introducing a single amino mutation. The aim of these calculations is to examine the difference in binding affinity or binding structure with the inhibitors between subtype B and subtype C HIV-1 PRs, and to clarify the change in mechanism for conferring drug resistance from the structural viewpoint. We particularly focus on (i) the role of the V82I mutation that is a common polymorphism seen in non-B subtype HIV-1 PR, and (ii) the effect of the D30N mutation in subtype C HIV-1 PR. Since subtype C HIV-1 PR has not sufficiently been surveyed in terms of the susceptibility for approved inhibitors and the emergence probability of drug resistant mutations, the information obtained in this study will give a hint to select the proper inhibitors for patients infected with subtype C HIV-1 and be helpful for the therapy for HIV-1 infectious disease in developing countries.

Methods

Molecular Dynamics (MD) Simulations. Minimizations and MD simulations were carried out using the Sander module of AMBER8.[27] The AMBER ff03 force field[28] was used as the parameters for proteins, ions, and water molecules. The general AMBER force field[29] was used as the parameters for ATV, NFV, and SQV. Our originally developed torsion parameters for the benzamide moiety in NFV, CA-CA-C -N and CA-CA-C -O, were applied.[30] Atom charges of inhibitors were determined from the electrostatic potential obtained from quantum chemical calculations, followed by the restrained electrostatic potential (RESP) fitting.[31] The stable structure of each inhibitor was determined through the geometry optimization at the HF/6-31G(d,p) level and, subsequently, the electrostatic potential was calculated at the B3LYP/cc-pVTZ level under the ether-phase condition. The quantum chemical calculations were executed with Gaussian03 program.[32]

We performed simulations of three clinically isolated subtype C HIV-1 PRs in complex with ATV, NFV, and SQV. These HIV-1 PRs were labeled as PR(#1), PR(#2), and PR(#3). Further, we labeled each complexes as PR(#1)-ATV, PR(#1)-NFV, PR(#1)-SQV, PR(#2)-ATV, PR(#2)-NFV, PR(#2)-SQV, PR(#3)-ATV, PR(#3)-NFV, and PR(#3)-SQV. Simulations of subtype B HIV-1 PR in complex with ATV, NFV, and SQV were also performed. This HIV-1 PR was labeled as PR(WT), and the complexes were as PR(WT)-ATV, PR(WT)-NFV, and PR(WT)-SQV. The sequence for HXB2[33] was applied to PR(WT). Simulation of PR(WT) containing the V82I mutation in complex with ATV was further performed. This HIV-1 PR was labeled as PR(V82I) and the complex of PR(V82I) and ATV was as PR(V82I)-ATV. Each initial structure for HIV-1

PR in complex with ATV, NFV and SQV was constructed from the atom coordinates of an X-ray crystal structure (Protein Data Bank (PDB) code, 2AQU, 1OHR, 1HXB)[21,34,35] and the respective mutations were introduced using the LEaP module of AMBER8. First, we downloaded the file of HIV-1 PR containing each inhibitor from PDB site. Second, the PDB file was edited to change the residue names of the mutated residues and to delete the description on the side-chain atoms of the mutated residues. Third, the coordinates of the side-chain atoms of the mutated residues were automatically generated by LEaP module. Fourth, each model was placed in a rectangular box filled with about 8000 TIP3P water molecules[36] with all of the crystal water molecules remaining. The cutoff distance for the long-range electrostatic and van der Waals energy terms was set to 12.0 Å. The expansion and shrinkage of all covalent bonds connecting to hydrogen atom were constrained using the SHAKE algorithm.[37] Periodic boundary conditions were applied to avoid the edge effect in all calculations.

Energy minimization was achieved in three steps. Initially, movement was allowed only for water molecules and ions. Next, inhibitor and mutated residues were allowed to move in addition to the water molecules and ions. In this step, the favorable configurations of the side chains of the mutated residues were obtained because steric collisions of them were minimized. Finally, all atoms were allowed to move freely. In each step, energy minimization was executed by the steepest descent method for the first 10 000 cycles and the conjugated gradient method for the subsequent 10 000 cycles. After a 0.1 ns heating calculation until 310 K using the NVT ensemble condition, a 3.0 ns equilibrating calculation was executed at 1.0 atm and at 310 K under the NPT ensemble condition with an integration time step of 2.0 fs. The calculation steps described above were performed both for two protonation states of catalytic residues, protonated D25/unprotonated D25′ and unprotonated D25/protonated D25′. Since the MD simulations showed no large fluctuations after about 2.5 ns equilibrating calculations for most of the complexes (Supporting Information Figures S2, S3), we evaluated the energies of the respective protonation states for each complex and selected the favorable one for the subsequent extended simulation. Additional 4.0 ns simulations were performed for the selected protonation state for each complex model. After 5.0 ns of the totally 7.0 ns equilibrating calculation, the MD simulations of all complexes showed little fluctuations (Supporting Information Figures S3, S4).

As for the complexes of PR(V82I)-ATV, the protonation state was determined in the same manner, using the simulation data for 3.0 ns. The 7.0 ns MD simulation was performed for the protonation state of unprotonated D25/protonated D25′. Additionally other 7.0 ns MD simulations were executed for protease only models, that is, PR(#1), PR(#2), and PR(#3) without inhibitors for the sake of comparison in structure.

Protonation State of Catalytic Residues. Protonation states of the catalytic aspartic acids D25 and D25′ of HIV-1 PR vary depending on the binding of inhibitor or the type of HIV-1 PR.[38] Thus, appropriate protonation states of the catalytic aspartic acids should be determined for each model. We considered two kinds of protonation states.[39−41] One is a combination of protonated D25/unprotonated D25′ states, and the other is the opposite combination. To determine the protonation states when each inhibitor is bound to each HIV-1 PR, the free energies of two kinds of protonation states were compared using calculation data obtained for the last 0.5 ns of 3.0 ns MD simulations. The free energies were calculated by the MM/PBSA method,[42,43] only for the inhibitor-PR complex without subtracting the values for inhibitor only and/or unbound PR. The same parameter set as used in the equilibrating calculations was adopted for computing electrostatic and van der Waals energy terms, and no cutoff was applied for the calculation. Since the dielectric constants for the interior of proteins is considered to be in the range of 2 to 4, the interior dielectric constant was set to 2.0.[41] The outside dielectric constant was set to 80.0. The pbsa module of AMBER8 was used to solve the Poisson-Boltzmman (PB) equation. PR(WT)-ATV, PR(WT)-SQV, PR(#1)-ATV, PR(#1)-NFV, PR(#1)-SQV, PR(#2)-ATV, PR(#2)-NFV, PR(#2)-SQV, PR(#3)-ATV, and PR(#3)-SQV have been found to favor the combination of protonated D25 and unprotonated D25′. The other complexes, PR(WT)-NFV and PR(#3)-NFV, prefer the combination of unprotonated D25 and protonated D25′ (Supporting Information Table S2).

Binding Free-Energy Calculation. The binding free energy[44] was calculated by the following equation

$$\Delta G_b = \Delta E_{int}^{cle} + \Delta E_{int}^{vdw} + \Delta G_{sol} - T\Delta S_v$$

where ΔG_b is the binding free energy in solution, ΔE_{int}^{cle} and ΔE_{int}^{vdw} are electrostatic and van der Waals interaction energies between an inhibitor and a protein, ΔG_{sol} is the solvation energy, and $T\Delta S_v$ is the contribution of vibrational entropy. The parameters for cutoff and dielectric constant were the same as those used in determining the protonation state. The snapshot structures were obtained every 10 ps from the trajectories of the last 1.0 ns simulation to calculate the terms ΔE_{int}^{ele}, ΔE_{int}^{vdw}, and ΔG_{sol}. The vibrational entropic term $T\Delta S_v$ was calculated using nmode module of AMBER9 at 310 K. The snapshot structures were collected every 50 ps from the last 1.0 ns trajectories to estimate $T\Delta S_v$. The modified GB model developed by Onufriev, Bashford, and Case[45] was used to calculate the solvation energy term. The MM/GBSA results were highly correlated with the MM/PBSA results, as we described previously.[30] To examine the energetic contribution of each residue, the energy without vibrational entropy was decomposed into the contribution from each individual residue by the MM/GBSA method.

Hydrogen Bond Criteria. The formation of a hydrogen bond was defined in terms of distance and orientation. The combination of donor D, hydrogen H, and acceptor A atoms with a D−H···A configuration was regarded as a hydrogen bond when the distance between donor D and acceptor A was shorter than 3.5 Å and the angle H−D−A was smaller than 60.0°.

Results

Sequence of HIV-1 PRs. We investigated three clinically isolated HIV-1s. Two of them, #1 and #2, were isolated from patients who had no experience in the treatment with any PR inhibitors. The other, #3, was isolated from a patient who failed in treatment with NFV. In this study, we labeled PRs of these clinically isolated HIV-1s as PR(#1), PR(#2), and PR(#3). The PR of subtype B HXB2 strain[33] was labeled as PR(WT).

The amino acid sequence of each PR was compared with that of PR(WT). PR(#1) has 14 amino acid mutations, T12S, K14R, I15V, L19I, K20R, M36I, N37D, R40K, R57K, L63P, H69K, V82I, L89M, and I93L, and PR(#2) has 13 amino acid mutations, T12P, I15V, K20R, M36I, N37K, R40N, R57K, Q61E, L63T, H69K, T74S, L89M, and I93L (Figure 1B). All these mutated residues are located at the nonactive site of PR, except for V82I of PR(#1). According to HIVdb of Stanford University,[23] both kinds of PRs have no primary mutations that

TABLE 1: Prediction of Susceptibility of the Inhibitors against the Clinically Isolated PRs[a]

	ATV	NFV	SQV
PR(#1)	susceptible	susceptible	susceptible
PR(#2)	slightly resistant	susceptible	susceptible
PR(#3)	slightly resistant	resistant	susceptible

[a] An inhibitor is judged to be susceptible, slightly resistant, or resistant when the binding free energy to a PR is lower than 2 kcal/mol, higher by 2−5 kcal/mol, or higher more than 5 kcal/mol compared with that of the wild-type PR, respectively.

are highly involved in the resistance against PR inhibitors. In contrast, PR(#3) has D30N, M46L, and N88D mutations that are primary mutations for drug resistance and also one secondary mutation L10F (Figure 1B). PR(#3) further contains nine amino acid mutations, T12S, I13V, I15V, L19I, E35D, M36V, R40K, H69K, and L89I. It has also already been reported that some mutations such as K20R, M36I/V, and H69K are related to resistance against PR inhibitors and these mutations are seen in polymorphisms.[22,23]

Computational Prediction of the Susceptibility of Inhibitors. The susceptibility of three kinds of inhibitors for the respective isolated HIV-1 PRs are judged from our simulation and summarized in Table 1. This judgment is based on the difference in binding free energy between the complexes with the isolated and wild-type PRs, which is presented as $\Delta\Delta G_b$ in Table2. In PR(#1), no energetic disadvantage is observed for NFV and SQV, and the energetic disadvantage is negligible for ATV compared to PR(WT). Therefore, all PR inhibitors are concluded to be susceptible to this variant. In PR(#2), an energetic disadvantage is observed only for the complex with ATV. Hence this mutant is judged to be weakly resistant only to ATV. PR(#3) shows the energetic disadvantage for ATV and NFV and is concluded to be resistant to these two inhibitors.

To support the judgment on the above prediction for susceptibility, the statistical analysis was carried out on the data for the binding energy calculation.[46] All the computed sampling data for the binding free energy were confirmed to be in the normal distribution. The f test with a significance level of 0.05 was performed to examine whether the data have the different variance or not between WT and each mutant for the respective inhibitors. Since the hypothesis was rejected for ATV and SQV for all the mutants, the computed sampling data for ATV and SQV were concluded to have the same variance between WT and each mutant. Therefore, Student's t test was applied for ATV and SQV, while Welch's t test was for NFV. According to the Student's t test with a significance level of 0.01, the means of the binding free energies for PR(#2)-ATV and PR(#3)-ATV were different from that for PR(WT)-ATV. For PR(#1)-ATV, the null hypothesis was not rejected even with a significance level of 0.05. The Welch's t test with a significance level of 0.01 indicated that the means of the binding free energies for PR(#1)-NFV and PR(#3)-NFV were different from that of PR(WT)-NFV. The Student's t test with a significance level of 0.01 suggested the difference of the means of the binding free energies for PR(#1)-SQV and PR(#2)-SQV compared to that for PR(WT)-SQV.

Binding Free Energy. Table 2 shows the detailed energy values in the computation of the binding free energy for the complexes of the respective PRs and three kinds of inhibitors. PR(#1) contains no primary mutations known for resistance to subtype B virus. The energy gain in $\Delta\Delta G_b$ is observed for NFV and SQV compared to PR(WT), and the calculation shows a slight energy loss for ATV. PR(#2) also contains no primary mutations and the energy gain in $\Delta\Delta G_b$ is seen only for NFV and SQV. Namely PR(#1) and PR(#2) show similar change in binding energy. Since PR(#3) was isolated from the patient who failed in the NFV treatment, it is straightforwardly understood that a large energy loss in $\Delta\Delta G_b$ is observed for the complex with NFV. PR(#3) also shows the energy loss for ATV, compared to that for PR(WT). For the purpose of examining the effect of single mutation, another MD simulation was performed for the PR in which an amino mutation of V82I was introduced in PR(WT). The complex of PR(V82I) and ATV showed no disadvantage in binding free energy compared to PR(WT).

Table 2 indicates that the electrostatic term mainly dominates the binding affinity of the complex while the vibrational entropic term has some degree of influence. As for the complexes showing the increase in binding affinity, the entropic term considerably contributes to the stability of the complex in PR(#1)-SQV and PR(#2)-SQV while van der Waals interaction enhances the stability of the complexes of PR(#1)-ATV and PR(#2)-NFV. The balance of the contributions of electrostatic, van der Waals, and entropic terms also varies for the complexes showing the decrease in binding affinity. PR(#2)-ATV exhibits energetic disadvantage in van der Waals term while PR(#3)-NFV and PR(#3)-SQV show the disadvantage in the electrostatic term. The standard deviation in binding free energy calculation is considerably large. Particularly the standard deviation of entropic term is large compared to $\Delta\Delta G_b$. Accordingly, we must be careful for the interpretation of the calculated binding free energy.

Hydrogen Bonding Networks. All direct and one-water-molecule-mediated hydrogen bonds between HIV-1 PR and inhibitor were examined for every complex (Supporting Information Tables S3−S6). To survey the formation of hydrogen bonds, we sampled 1000 snapshot structures from the trajectory of the last 1.0 ns MD simulation. In all cases, the hydroxyl group existing at the center of the inhibitors makes a direct hydrogen bond to D25 or D25′ of PR. I50 or I50′ residue of PRs keeps an one-water-molecule-mediated hydrogen bond to the inhibitor. Furthermore, different hydrogen bond networks are observed among PR(#1), PR(#2), PR(#3), and PR(WT) in complex with each inhibitor.

Direct hydrogen bonds from ATV are connected to D29′ and G48′ in PR(WT)-ATV. PR(#1) hardly has the direct hydrogen bond to ATV. PR(#2) keeps the hydrogen bond to G48′ and D29′, while the hydrogen bond to D29′ is weakened. PR(#3) loses both hydrogen bonds seen in PR(WT), whereas a new hydrogen bond to D29 appears. As for NFV, PR(WT) has a direct hydrogen bond between the side chain of D30 and NFV. This hydrogen bond is kept in PR(#1)-NFV and PR(#2)-NFV. Although D30 was substituted for N30 in PR(#3), the side chain of N30 still keeps hydrogen bond to NFV. As for SQV, G48 in PR(WT) forms a direct hydrogen bond to SQV. In PR(#1)-SQV, G48 and D30 make direct hydrogen bonds to SQV. G48 in PR(#2) keeps a hydrogen bond to SQV as well as PR(WT). In contrast, the hydrogen bond from N2 of SQV disappears in PR(#3).

Change in Conformation of PRs and Inhibitors. The averaged structures of PR and inhibitor in each model were compared with those for the complex in PR(WT). The averaged structure was obtained from 1000 snapshot structures during the last 1.0 ns MD simulation. To compare the structure with that of PR(WT), the averaged structure of each mutant was superimposed on PR(WT) in respect of atom coordinates of N, Cα, and C atoms and, then, the root-mean-square deviation

TABLE 2: Binding Free Energy of the Complex of HIV-1 PR and Its Inhibitor

	ΔG_{int}^{ele}(kcal/mol)	ΔG_{int}^{vdw}(kcal/mol)	ΔG_{sol} (kcal/mol)	$-T\Delta S$ (kcal/mol)	ΔG_b (kcal/mol)	$\Delta\Delta G_b$ (kcal/mol)[a]
PR(WT)-ATV	−15.7 ± 1.7	−74.1 ± 3.5	11.6 ± 1.5	26.2 ± 7.5	−52.0	
PR(WT)-NFV	−24.2 ± 2.1	−66.9 ± 4.2	12.5 ± 1.7	29.1 ± 6.8	−49.5	
PR(WT)-SQV	−15.1 ± 2.9	−70.1 ± 4.3	10.0 ± 1.3	31.1 ± 6.0	−44.1	
PR(#1)-ATV	−12.8 ± 2.2	−79.9 ± 3.0	12.9 ± 1.1	28.8 ± 8.6	−51.0	+1.0
PR(#1)-NFV	−18.4 ± 3.0	−72.2 ± 3.4	11.9 ± 1.5	25.0 ± 9.0	−53.7	−4.2
PR(#1)-SQV	−21.7 ± 4.2	−72.4 ± 3.9	13.6 ± 1.7	27.0 ± 9.6	−53.5	−9.4
PR(#2)-ATV	−17.7 ± 3.6	−70.5 ± 4.1	12.8 ± 1.9	27.0 ± 5.8	−48.4	+3.6
PR(#2)-NFV	−20.0 ± 5.9	−69.1 ± 2.8	13.0 ± 1.2	26.2 ± 7.4	−49.9	−0.4
PR(#2)-SQV	−16.6 ± 3.5	−67.9 ± 4.7	10.6 ± 1.8	25.6 ± 8.6	−48.3	−4.2
PR(#3)-ATV	−12.2 ± 2.1	−76.5 ± 3.6	12.0 ± 1.2	28.2 ± 7.4	−48.5	+3.5
PR(#3)-NFV	−13.1 ± 1.9	−65.5 ± 3.2	10.5 ± 1.2	25.3 ± 6.6	−42.8	+6.7
PR(#3)-SQV	−13.0 ± 2.5	−71.5 ± 3.9	9.0 ± 0.9	30.6 ± 6.2	−44.9	−0.8
PR(V82I)-ATV	−24.4 ± 2.4	−80.8 ± 4.7	15.4 ± 1.5	23.6 ± 6.9	−66.2	−13.2

[a] Difference from PR(WT).

TABLE 3: Genotype Assay of Clinically Isolated PRs in Complex with Each Inhibitor

	ATV	NFV	SQV
PR(#1)	susceptible[a]	susceptible	susceptible
PR(#2)	susceptible	susceptible	susceptible
PR(#3)	intermediate resistance[b]	high-level resistance[c]	low-level resistance[d]

[a] Virus of this category hardly shows the reduction in susceptibility to the drug. [b] Virus of this category shows certain degree of drug resistance between the low-level and the high-level resistances. [c] Virus of this category shows the highest levels of the in vitro drug resistance and/or the patients infected with viruses of this category generally have little or no virologic response to treatment with the drug. [d] Virus of this category reduces the in vitro susceptibility to the drug and/or the patients with viruses of this category may have a suboptimal virologic response to treatment.

(rmsd) value was calculated (Figure 2A). Since the residues located at the outer part of PR largely fluctuate (Supporting Information Figure S6), we focused only on the structural change of the residues located near the active site of HIV-1 PRs. A prominent structural change is seen in the complexes of PR(#1)-ATV, PR(#1)-NFV, PR(#2)-NFV, and PR(#3)-NFV at the 80s loop which corresponds to 80−84th residues of PR. PR(#1)-ATV and PR(#3)-ATV show a structural change at the flap region. No significant changes are observed for the other complexes around the binding pocket. In contrast, the change in binding pose is more clearly observed for the inhibitors. In the complexes of PR(#1), the ring parts of the respective inhibitors, 3′-phenylpyridine group in ATV and phenylsulfanyl group in NFV, show large deviations, compared with that of PR(WT). These large structural deviations are also seen in the complexes of PR(#2). PR(#3) shows the deviation not only at the ring part but also for the whole part of all the inhibitors. The quinoline group in SQV shows a considerable deviation in PR(#3), while PR(#1) and PR(#2) has little change compared with PR(WT).

Discussion

PR(#1) and PR(#2). Both PR(#1) and PR(#2) were derived from the patients who were naive for the treatment with PR inhibitors. The polymorphisms at the 20th, 36th, 69th, and 93rd residues are commonly seen in both sequences of PR(#1) and PR(#2). All these amino acid mutations were reported to be involved in drug resistance of subtype B HIV-1 PR.[14−22] It is important to note that these mutations are not the primary mutation for drug resistance but the secondary mutation accompanying with some primary mutations. Hence, judging from the knowledge accumulated on subtype B PR, these mutations would not cause the drug resistance by themselves. Indeed, according to HIVdb, the genotype assay web service of Stanford University,[23] both of PR(#1) and PR(#2) were judged not to cause the resistance against the approved PR inhibitors (Table 3). Genotype assay is the prediction method for drug resistance based only on the sequence of the virus and sometimes used in the clinical scene. The calculated binding free energy of the present MD simulation has suggested an almost similar conclusion that NFV and SQV are almost effective for PR(#1) and PR(#2) as well as PR(WT). Only the assessment for PR(#2)-ATV complex is different (Table 1).

V82I Mutation. Our simulation suggests that PR(#2) is weakly resistant only for ATV (Table 1). It is informative to clarify the cause for the difference in efficacy of ATV between PR(#1) and PR(#2). A comparison in the amino sequence between PR(#1) and PR(#2) shows that V82I and V63P mutations appear only in PR(#1). Since the 82nd residue is located at the inhibitor-binding site of PR and has direct interaction with the PR inhibitors, V82I may have some degree of influence on the binding affinity between PR and its inhibitor. The 82nd residue is, further, known as a key residue relating to the recognition of substrate.[22,47−49] Accordingly, it will be important to examine the effect of the V82I mutation on the PR-ATV complex. Several previous studies with X-ray crystal analysis suggested that the 82nd residue is located at the vicinity of ring part of ATV (3′-phenylpyridil group).[21,34,35] Our present MD simulation indicates that the V82I mutation causes structural change not only in PR but also in ATV (Figure 2), which leads the stable binding pose of ATV different from that in PR(WT). In PR(WT), the side chain of V82 is positioned with facing to the inner side of the binding pocket (Figure 3A). In contrast, the side chain of I82 faces opposite to the binding pocket (Figure 3B). Furthermore, 3′-phenylpyridyl group of ATV occupies the different space compared to PR(WT). 3′-phenylpyridyl group interacts with the flap region around the 50th residues in PR(WT), while this group is shifted toward I84 in PR(#1). This shift will increase the van der Waals interaction between PR and ATV (Table 2) and, further, induces the formation of hydrogen bond between D25 and ATV (Supporting Information, Tables S3 and S4). The binding free energy for the ATV-PR complex was decomposed into the contributions from the respective residues (Supporting Information, Figure S8). A comparison of the decomposed binding energies of PR(#1), PR(#2), PR(#3) with PR(WT) indicated that noticeable energy loss appears around the residues of A28′, D29′, G48′, and T80′. Inversely, energy gain is observed at the residue of R8 and D29. All these amino residues are located at the active site, and the

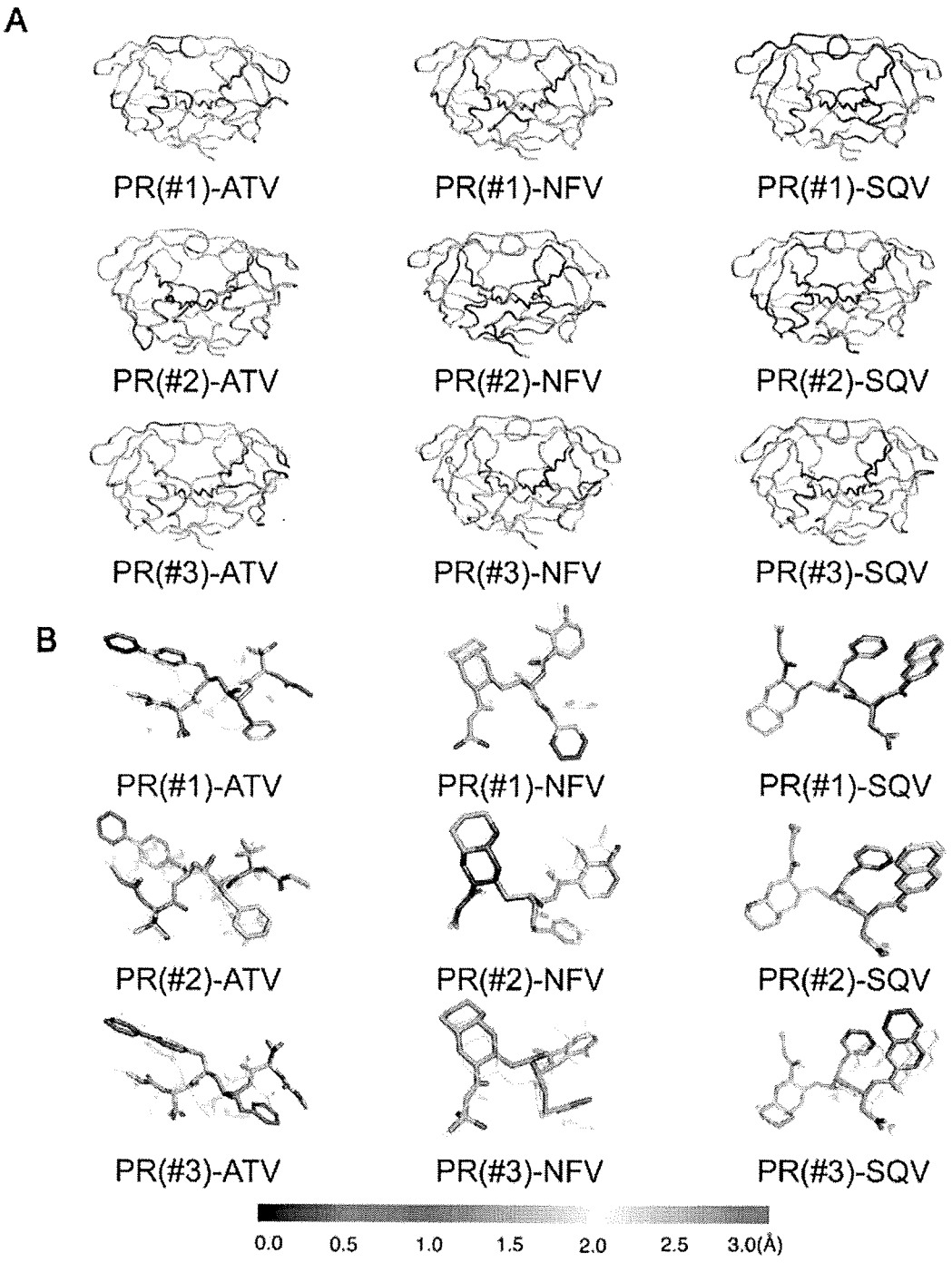

Figure 2. (A) Three-dimensional plot of rmsd of the average structure of each PR measured from PR(WT). PRs are shown in the colored tube representation. (B) Three-dimensional plot of rmsd of the average structure of each PR inhibitor measured from PR(WT). Inhibitors are shown in the colored stick representation. The color means the magnitude of rmsd shown in the bottom bar. The superimposed gray tubes in A and sticks in B represent the structure in PR(WT).

energy changes were mainly caused by the displacement of the binding position of ATV.

In order to examine whether the above structural changes are indeed caused by the V82I mutation, we executed another 3.0 ns MD simulation on PR(V82I)-ATV complex, where PR(V82I) model was constructed by introducing the V82I mutation into PR(WT). This simulation on PR(V82I) shows that the side chain of V82I faces opposite to the binding pocket and 3′-phenylpyridyl group of ATV is shifted toward I84 (Figure 3C). Our energy calculation shows no loss in binding free energy both in PR(#1) and PR(V82I) (Table 2). That is, the V82I mutation causes the structural change, but no decrease in binding affinity. In contrast to PR(#1), PR(#2) does not contain the V82I mutation and PR(#2)-ATV complex shows the loss in binding free energy compared to PR(WT). In the binding structure of the PR(#2)-ATV complex, 3′-phenylpyridyl group of ATV is slightly shifted as well as PR(#1), but the 82nd residue is not completely shifted from the original position (Figure 3D). Because of the slight positional shift, 3′-phenylpyridyl group still keep the interaction with the flap region of PR in a similar manner with PR(WT). This halfway position of ATV is energetically unfavorable. Therefore, we can conclude that the V82I mutation causes the alteration of the position of side chain of I82 and the shift of ring part of ATV toward 80′ loop. This

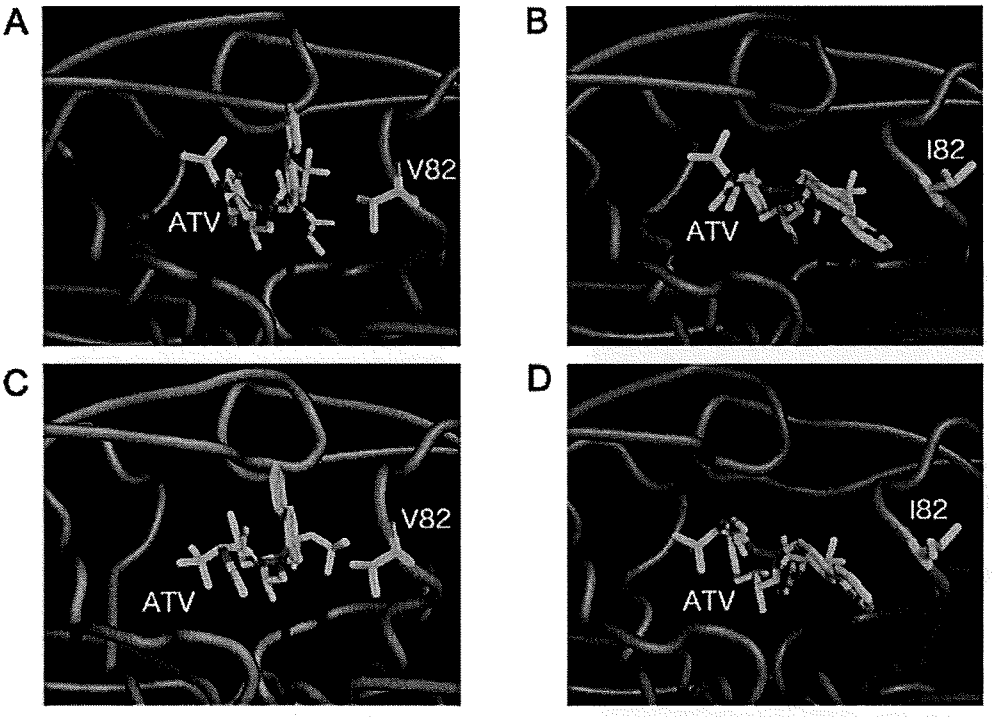

Figure 3. Structure of ATV and the 82nd residue in each model. ATV and the residue are shown by sticks and PR is by tubes. (A) PR(WT)-ATV, (B) PR(#1)-ATV, (C) PR(#2)-ATV, (D) PR(V82I)-ATV.

shift keeps the energetic stability of the complex of PR and ATV. The presence of the V82I mutation exerts a strong influence on the binding with ATV and one of the prominent characteristics for subtype C HIV-1 PR.

PR(#3). Since PR(#3) was derived from the patient who failed in the treatment with NFV, PR(#3) contains mutations known to confer resistance against NFV. The genotype assay based on the HIVdb of Stanford University suggested the resistance to NFV and, further, indicated the resistance to ATV and SQV. The calculated binding free energy in our present work gave a similar conclusion. That is, a large loss in binding free energy is observed for the PR(#3)-NFV complex, compared with PR(WT), and the energy loss is also seen for the complexes with ATV. The D30N mutation appearing in PR(#3) is well-known as the primary mutation causing the resistance against NFV and frequently seen in the patient who was infected with subtype B HIV-1 and failed in the treatment with NFV.[22,50] In subtype B HIV-1 PR, the break of the hydrogen bond between the side chain of N30 and NFV due to the D30N mutation is the main reason for causing resistance to NFV.[30,51,52] The hydrogen bond between the side chain of N30 and NFV is, however, maintained in PR(#3) in contrast with the subtype B D30N-mutated PR (Supporting Information, Tables S3 and S6). As our previous simulation on the D30N/M36 V doubly mutated subtype B PR suggested, the M36 V mutation in PR(#3), which is also reported to be involved in resistance to NFV,[13] will induce the formation of hydrogen bonds between NFV and N30.[52] Therefore, the M36 V mutation is effective for keeping the hydrogen bond both in subtype B and subtype C PRs. The hydrogen bond was observed to disappear for a while for 7.0 MD simulation and the m-phenyl group of NFV was occasionally change its position in the PR(#3)-NFV complex. This means that the chain of N30 cannot make a strong hydrogen bond with m-phenyl group of NFV compared to D30. This will be a reason for low binding affinity of NFV to PR(#3).

In the PR(#3)-ATV complex, the binding free energy was diminished compared to PR(WT) due to the shift of the binding position of ATV. This position shift is reflected in the disappearance of hydrogen bonds seen in PR(WT) and the appearance of another direct hydrogen bond between D29 and O2 of ATV (Supporting Information, Table S6). No energy loss was observed in the PR(#3)-SQV complex. This result is compatible with the findings that PR(#3) contains few mutations related to SQV resistance.[22]

D30N Mutation. PR(#3) is the subtype C HIV-1 PR containing the D30N mutation. The appearance of the D30N mutation was, however, reported to be rare in the subtype C HIV-1 showing the drug resistance to NFV.[13,18,25,26] Therefore, it is informative to clarify the reason why the D30N mutation rarely appears in subtype C HIV-1 PR from the structural viewpoint. Some experimental findings indicated that the rare appearance of the D30N mutation in subtype C HIV-1 PR is closely related to the replication ability of the virus.[25,26] The replication ability of subtype C HIV-1 containing the D30N/N88D mutation was lower than the variant containing the L90 M mutation, though the D30N/N88D and L90 M mutations are known as the primary mutation conferring resistance against NFV in subtype B HIV-1.[26] It has been reported that the 29th and 87th residues in PR are related to the stability of dimer formation.[53,54] Considering this finding, we paid our attention to the structure of the 29th and 87th residues in the PR(#3)-NFV complex. If the structural stability of HIV-1 PR is reduced, the enzymatic activity of PR to cleave the peptide linkage of substrate will be seriously lowered. The low enzymatic activity will lead to the decrease in replication ability. It was found that the side chain of D29 was shifted toward the inner side of the binding pocket in PR(#3)-NFV, compared to PR(WT)-NFV (Figure 4A,B). Further, the side chain of R87 was displaced opposite to the binding pocket. Our previous simulations suggested that the mutation at the 36th residue influences the geometry of D29.[51] Hence, in order to further examine the influence of the M36 V mutation on the 29th and 87th residues, we have performed another MD simulation on the complex of NFV and PR(WT) containing the D30N/M36 V mutation. This

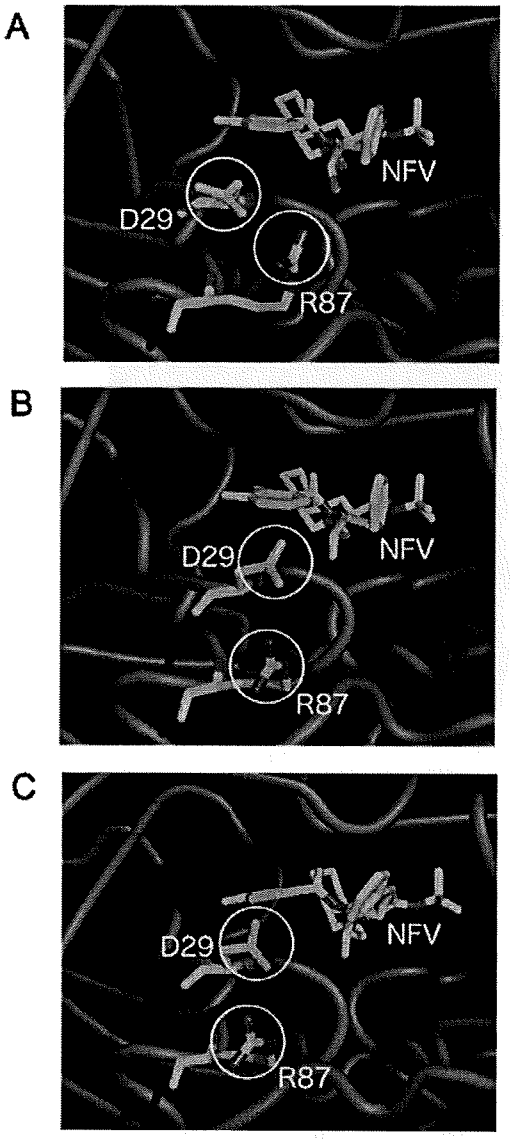

Figure 4. Structure of NFV and the 29th and 87th residues. ATV and the residues are shown by sticks and PR is by tubes. (A) PR(WT)-NFV, (B) PR(#3)-NFV, (C) PR(D30N/M36 V)-NFV.

simulation showed a structural change at the side chains of the 29th and 87th residues as well as PR(#3) (Figure 4C). Accordingly, we conclude that the D30N/M36 V mutation causes the position shift of the side chains of the 29th and 87th residues in the subtype C HIV-1 PR, which induces the structural instability of HIV-1 PR and leads to the lowering of the enzymatic activity of PR. This low enzymatic activity results in the decrease of the replication ability of HIV-1. Since the replication rate of subtype C virus containing the D30N mutation is low, most of the subtype C HIV-1s resistant to NFV rarely contain the D30N mutation.

Overall Picture of the Structure of Subtype C HIV-1 Protease. On the basis of the results of the present MD simulation, we have proposed the influence of polymorphisms of subtype C HIV-1 PR on the susceptibility of drugs. The discussion was mainly developed from the viewpoint of complex structure of PR and inhibitor. A comparison of structures of PRs with and without the inhibitors clearly shows the difference at the flap region (Supporting Information, Figure S7). The flap tips were displaced upward due to the association with the inhibitor in every complex. This displacement is particularly evident in PR(#1) and PR(#2). PR(#3) markedly shows the displacement at the flap elbow and fulcrum loop (Supporting Information, Figure S6).

The X-ray crystal analysis is one of the most powerful techniques to investigate the structure of protein. Recently a crystallization of the subtype C PR was achieved by Coman et al.[54,55] Their first report provided the information on the X-ray crystal structure of the subtype C PR complexed with two kinds of inhibitors, indinavir (IDV) and NFV.[55] Their second report gave a comparison between the inhibitor-unbound subtype C and B PRs.[56] The unbound subtype C PR exhibited a larger distance between the two flap tips, a downward displacement of the 36−41's loop, and an increased thermal stability of the 10s loop, compared with subtype B. The increase of the distance of the flap tips is seen in the PR(#1)-ATV and PR(#3)-NFV complexes in our present simulation and the downward displacement of the 36−41's loop is obvious in the PR(#1)-ATV, PR(#2)-NFV, PR(#3)-ATV and PR(#3)-SQV complexes (Figure 2). The increase of stability of the 10s loop is observed in PR(#1)-SQV, PR(#3)-NFV, and PR(#3)-SQV (Supporting Information, Figure S6). Therefore, some of the structural characteristics are compatible with between the X-ray crystal structure and our simulation results. Our calculation will also suggest the drug efficacy of the respective inhibitors on the clinically isolated subtype C PRs. Since structural findings give an insight into the drug resistance, viral fitness, and the response to therapy, it will be required to accumulate much information about the complex structures of the nonsubtype B HIV-1 PRs and inhibitors both from experimental and theoretical approaches. The accumulated data will be useful for the proper choice of inhibitors, which enhances the performance of anti-HIV therapy for the patients infected with the nonsubtype B virus.

Conclusion

MD simulations on the complexes of subtype C HIV-1 PR and three kinds of approved inhibitors were carried out to investigate the influence of natural polymorphisms of subtype C on the change in binding affinity with the inhibitors. The simulation suggested that ATV occasionally decreases the susceptibility to the subtype C HIV-1 PRs. The presence of the V82I polymorphism affects the structural stability of the complex, which is related to the decrease of the susceptibility of ATV. The subtype C HIV-1 PR containing the D30N mutation will confer drug resistance even for the variant containing the M36 V mutation. This is a difference from the subtype B HIV-1 PR. Our MD simulation provided the reason why the emergence rate of the D30N mutation is low for subtype C HIV-1 PR. The low emergence rate is interpreted as a result from the decrease of HIV-1 replication ability of the D30N containing variant.

Acknowledgment. This work was supported by Grant-in-Aid for Scientific Research (C) from Japan Society for the Promotion of Science (JSPS) and by a Health and Labor Science Research Grant for Research on Publicly Essential Drugs and Medical Devices from the Ministry of Health and Labor of Japan. One of the authors (H.O.) gratefully acknowledges the postdoctoral research fellowship from JSPS. A part of this work was also supported by a grant from the Futaba Electronics Memorial Foundation.

Supporting Information Available: Description on the amino sequence of the isolated samples, a list of hydrogen bond networks, the determination of protonation states of catalytic

aspartic acids, B-factors of the respective residues in simulation, comparison of structures with and without the inhibitors, rmsd plots during MD simulations, and the results of principal component analyses were provided. This material is available free of charge via the Internet at http://pubs.acs.org.

References and Notes

(1) Joint United Nations Programme on HIV/AIDS (UNAIDS). 2007 AIDS Epidemic Update UNAIDS. 2007.

(2) Kräusslich, H. G.; Wimmer, E. *Annu. Rev. Biochem.* **1988**, *57*, 701.

(3) Kohl, N. E.; Emini, E. A.; Schleif, W. A.; Davis, L. J.; Heimbach, J. C.; Dixon, R. A.; Scolinick, E. M.; Sigal, I. S. *Proc. Natl. Acad. Sci. U.S.A.* **1988**, *85*, 4686.

(4) Craig, J. C.; Duncan, I. B.; Hockley, D.; Grief, C.; Roberts, N. A.; Mills, J. S. *Antiviral Res.* **1991**, *16*, 295.

(5) Vacca, J. P.; Dorsey, B. D.; Schleif, W. A.; Leven, R. B.; McDaniel, S. L.; Darke, P. L.; Zugay, J.; Quintero, J. C.; Blahy, O. M.; Roth, E.; Sardana, V. V.; Schlabach, A. J.; Graham, P. I.; Condra, J. H.; Gotlib, L.; Holloway, M. K.; Lin, J.; Chen, L.-W.; Vastag, K.; Ostvic, D.; Anderson, P. S.; Emini, E. A.; Huff, J. R. *Proc. Natl. Acad. Sci. U.S.A.* **1994**, *91*, G4096.

(6) Kempf, D. J.; Marsh, K. C.; Denissen, J. F.; McDonald, E.; Vasavanonda, S.; Flentga, C. A.; Green, B. E.; Fino, L.; Park, C. H.; Kong, X.; Wideburg, N. E.; Saldivar, A.; Ruiz, L.; Kati, W. M.; Sham, H. L.; Robins, T.; Stewart, K. D.; Hsu, A.; Plattner, J. J.; Leonard, J. M.; Norbeck, D. W. *Proc. Natl. Acad. Sci. U.S.A.* **1995**, *92*, 2484.

(7) Livington, D. J.; Pazhanisamy, S.; Porter, D. J.; Partaledis, J. A.; Tung, R. D.; Painter, G. R. *J. Infect. Dis.* **1995**, *172*, 1238.

(8) Patick, A. K.; Mo, H.; Markowitz, M.; Appelt, K.; Wu, B.; Musick, L.; Kalish, V.; Kaldor, S.; Reich, S.; Ho, D.; Webber, S. *Antimicrob. Agents Chemother.* **1996**, *40*, 292 Erratum, 40, 1575.

(9) Carrillo, A.; Stewart, K. D.; Sham, H. L.; Norbeck, D. W.; Kohlbrenner, W. E.; Leonard, J. M.; Kempf, D. J.; Molla, A. J. *J. Virol.* **1998**, *72*, 7532.

(10) Robinson, B. S.; Riccardi, K. A.; Gong, Y. F.; Guo, Q.; Stock, D. A.; Blair, W. S.; Terry, B. J.; Deminie, C. A.; Djang, F.; Colonno, R. J.; Lin, P. F. *Antimicrob. Agents Chemother.* **2000**, *44*, 2093.

(11) Larder, B. A.; Hertogs, K.; Bloor, S.; van den Eynde, C.; DeCian, W.; Wang, Y.; Freimuth, W. W.; Tarpley, G. *AIDS* **2000**, *14*, 1943.

(12) Koh, Y.; Nakata, H.; Maeda, K.; Ogata, H.; Bilcer, G.; Devasamudram, T.; Kincaid, J. F.; Boross, P.; Wang, Y. F.; Tie, Y.; Volarath, P.; Gaddis, L.; Harrison, R. W.; Weber, I. T.; Ghosh, A. K.; Mitsuya, H. *Antimicrob. Agents Chemother.* **2003**, *47*, 3123.

(13) Kantor, R.; Katzenstein, D. A.; Efron, B.; Carvalho, A. P.; Wynhoven, B.; Cane, P.; Clarke, J.; Sirivichayakul, S.; Soares, M. A.; Snoeck, J.; Pillay, C.; Rudich, H.; Rodrigues, R.; Holguin, A.; Ariyoshi, K.; Bouzas, M. B.; Cahn, P.; Sugiura, W.; Soriano, V.; Brigido, L. F.; Grossman, Z.; Morris, L.; Vandamme, A. M.; Tanuri, A.; Phanuphak, P.; Weber, J. N.; Pillay, D.; Harrigan, P. R.; Camacho, R.; Schapiro, J. M.; Shafer, R. W. *PLoS Med.* **2005**, *2*, 325.

(14) Cornelissen, M.; van den Burg, R.; Zorgdrager, F.; Lukashov, V.; Goudsmit, J. *J. Virol.* **1997**, *71*, 6348.

(15) Pieniazek, D.; Rayfield, M.; Hu, D. J.; Nkengasong, J.; Wiktor, S. Z.; Downing, R.; Biryahwaho, B.; Mastro, T.; Tanuri, A.; Soriano, V.; Lal, R.; Dondero, T. *AIDS* **2000**, *14*, 1489.

(16) Vergne, L.; Peeters, M.; Mpoudi-Ngole, E.; Bourgeois, A.; Liegeois, F.; Toure-Kane, C.; Mboup, S.; Mulanga-Kabeya, C.; Saman, E.; Jourdan, J.; Reynes, J.; Delaporte, E. *J. Clin. Microbiol.* **2000**, *38*, 3919.

(17) (a) Grossman, Z.; Vardinon, N.; Chemtob, D.; Alkan, M. L.; Bentwich, Z.; Burke, M.; Gottesman, G.; Istomin, V.; Levi, I.; Maayan, S.; Shahar, E.; Schapiro, J. M. *AIDS* **2001**, *15*, 1453. (b) Grossman, Z.; Vardinon, N.; Chemtob, D.; Alkan, M. L.; Bentwich, Z.; Burke, M.; Gottesman, G.; Istomin, V.; Levi, I.; Maayan, S.; Shahar, E.; Schapiro, J. M. *AIDS* **2001**, *15*, 2209.

(18) Cane, P. A.; de Ruiter, A.; Rice, P.; Wiselka, M.; Fox, R.; Pillay, D. *J. Clin. Microbiol.* **2001**, *39*, 2652.

(19) Zhong, P.; Kang, L.; Pan, Qichao.; Koings, F.; Burda, S.; Ma, L.; Xue, Y.; Zheng, X.; Jin, Z.; Nyambi, P. *JAIDS, J. Acquired Immune. Defic. Syndr.* **2003**, *34*, 91.

(20) Ariyoshi, K.; Matsuda, M.; Miura, H.; Tateishi, S.; Yamada, K.; Sugiura, W. *AIDS, J. Acquired Immune. Defic. Syndr.* **2003**, *33*, 336.

(21) Clemente, J. C.; Coman, R. M.; Thiaville, M. M.; Janka, L. K.; Jeung, J. A.; Nukoolkarn, S.; Govindasamy, L.; Agbandje-McKenna, M.; McKenna, R.; Leelamanit, W.; Goodenow, M. M.; Dunn, B. M. *Biochemistry* **2006**, *45*, 5468.

(22) Johnson, V. A.; Brun-Vézinet, F.; Clotet, N.; Günthard, H. F.; Kuritzkes, D. R.; Pillay, D.; Schapiro, J. M.; Richman, D. D. *Top. HIV Med.* **2008**, *16*, 62.

(23) Rhee, S.-Y.; Gonzales, M. J.; Kantor, R.; Betts, B. J.; Ravela, J.; Shafer, R. W. *Nucleic Acids Res.* **2003**, *31*, 298.

(24) Velazquez-Campoy, A.; Todd, M. T.; Vega, S.; Freire, E. *Proc. Natl. Acad. Sci. U.S.A.* **2001**, *98*, 6062.

(25) Grossman, Z.; Paxinos, E. E.; Averbuch, D.; Maayan, S.; Parkin, N. T.; Dan, E.; Margalit, L.; Valery, I.; Shaked, Y.; Mendelson, E.; Ram, D.; Petropoulos, C. J.; Schapiro, J. M. *Antimicrob. Agents Chemother.* **2004**, *48*, 2159.

(26) Gonzalez, L. M. F.; Brindeiro, R. M.; Aguiar, R. S.; Pereira, H. S.; Abreu, C. M.; Soares, M. A.; Tanuri, A. *Antimicrob. Agents Chemother.* **2004**, *48*, 3552.

(27) Case, D. A.; Darden, T. A.; Cheatham, T. E., III; Simmerling, C. L.; Wang, J.; Duke, R. E.; Luo, R.; Merz, K. M.; Wang, B.; Pearlman, D. A.; Crowly, M.; Brozell, S.; Tsui, V.; Gohlke, H.; Mongan, J.; Hornak, V.; Cui, G.; Beroza, P.; Schafmeister, C.; Caldwell, J. W.; Ross, W. S.; Kollman, P. A. *Amber 8*; University of California: San Francisco, CA, 2004.

(28) Duan, Y.; Wu, C.; Chowdhury, S.; Lee, M. C.; Xiong, G.; Zhang, W.; Yang, R.; Cieplak, P.; Luo, R.; Lee, T. *J. Comput. Chem.* **2003**, *24*, 1999.

(29) (a) Wang, J.; Wolf, R. M.; Caldwell, J. W.; Kollman, P. A.; Case, D. A. *J. Comput. Chem.* **2004**, *25*, 1157. (b) Wang, J.; Wolf, R. M.; Caldwell, J. W.; Kollman, P. A.; Case, D. A. *J. Comput. Chem.* **2005**, *26*, 114.

(30) Ode, H.; Matsuyama, S.; Hata, M.; Hoshino, T.; Kakizawa, J.; Sugiura, W. *J. Med. Chem.* **2007**, *50*, 1768.

(31) Cieplak, P.; Cornell, W. D.; Bayly, C.; Kollman, P. A. *J. Comput. Chem.* **1995**, *16*, 1357.

(32) Frisch, M. J. Trucks, G. W.; Schlegel, H. B.; Scuseria, G. E.; Robb, M. A.; Cheeseman, J. R.; Montgomery, J. A., Jr.; Vreven, T.; Kudin, K. N.; Burant, J. C.; Millam, J. M.; Iyengar, S. S.; Tomasi, J.; Barone, V.; Mennucci, B.; Cossi, M.; Scalmani, G.; Rega, N.; Petersson, G. A.; Nakatsuji, H.; Hada, M.; Ehara, M.; Toyota, K.; Fukuda, R.; Hasegawa, J.; Ishida, M.; Nakajima, T.; Honda, Y.; Kitao, O.; Nakai, H.; Klene, M.; Li, X.; Knox, J. E.; Hratchian, H. P.; Cross, J. B.; Bakken, V.; Adamo, C.; Jaramillo, J.; Gomperts, R.; Stratmann, R. E.; Yazyev, O.; Austin, A. J.; Cammi, R.; Pomelli, C.; Ochterski, J. W.; Ayala, P. Y.; Morokuma, K.; Voth, G. A.; Salvador, P.; Dannenberg, J. J.; Zakrzewski, V. G.; Dapprich, S.; Daniels, A. D.; Strain, M. C.; Farkas, O.; Malick, D. K.; Rabuck, A. D.; Raghavachari, K.; Foresman, J. B.; Ortiz, J. V.; Cui, Q.; Baboul, A. G.; Clifford, S.; Cioslowski, J.; Stefanov, B. B.; Liu, G.; Liashenko, A.; Piskorz, P.; Komaromi, I.; Martin, R. L.; Fox, D. J.; Keith, T.; AlLaham, M. A.; Peng, C. Y.; Nananyakkara, A.; Challacombe, M.; Gill, P. M. W.; Johnson, B.; Chen, W.; Wong, M. W.; Gonzalez, C.; Pople, J. A. *Gaussian 03*; Gaussian, Inc.: Wallingford, CT, 2004.

(33) Ratner, L.; Haseltine, W.; Patarca, R.; Livak, K. J.; Starcich, B.; Josephs, S. F.; Doran, E. R.; Rafalski, J. A.; Whitehorn, E. A.; Baumeister, K.; Ivanoff, L.; Petteway, S. R., Jr.; Pearson, M. L.; Lautenberger, J. A.; Papas, T. S.; Ghrayebparallel, J.; Changparallel, N. T.; Gallo, R. C.; Wong-Staal, F. *Nature* **1985**, *313*, 277.

(34) Kaldor, S. W.; Kalish, V. J.; Davies, J. F.; Shetty, B. V.; Fritz, J. E.; Appelt, K.; Burgess, J. A.; Campanale, K. M.; Chirgadze, N. Y.; Clawson, D. K.; Dressman, B. A.; Hatch, S. D.; Khalil, D. A.; Kosa, M. B.; Lubbehusen, P. P.; Muesing, M. A.; Patrick, A. K.; Reich, S. H.; Su, K. S.; Tatlock, J. H. *J. Med. Chem.* **1997**, *40*, 3979.

(35) Krohn, A.; Redshaw, S.; Ritchie, J. C.; Graves, B. J.; Hatada, M. H. *J. Med. Chem.* **1991**, *34*, 3340.

(36) Jorgensen, W. L.; Chandrasekhar, J.; Madura, J. D.; Impey, R. W.; Klein, M. L. *J. Chem. Phys.* **1983**, *79*, 926.

(37) Ryckaert, J.-P.; Ciccotti, G.; Berendsen, H. J. C. *J. Comput. Phys.* **1977**, *23*, 327.

(38) Zoete, V.; Michielin, O.; Karplus, M. *J. Mol. Biol.* **2002**, *315*, 21.

(39) Roberts, N. A.; Martin, J. A.; Kinchington, D.; Broadhurst, A. V.; Craig, J. C.; Duncan, I. B.; Galpin, S. A.; Handa, B. K.; Kay, J.; Krohn, A.; Lambert, R. W.; Merrett, J. H.; Millis, J. S.; Parkes, K. E. B.; Redshaw, S.; Ritchie, A. J.; Taylor, D. L.; Thomas, G. L.; Machin, P. J. *Science* **1990**, *248*, 358.

(40) Okimoto, N.; Tsukui, T.; Hata, M.; Hoshino, T.; Tsuda, M. *J. Am. Chem. Soc.* **1999**, *121*, 7349.

(41) Wang, W.; Kollman, P. A. *J. Mol. Biol.* **2000**, *303*, 567.

(42) Srinivasan, J.; Cheatham, T. E., III; Kollman, P.; Case, D. A. *J. Am. Chem. Soc.* **1998**, *120*, 9401.

(43) Kollman, P. A.; Massova, I.; Reyes, C.; Kuhn, B.; Huo, S.; Chong, L.; Lee, M.; Lee, T.; Duan, Y.; Wang, W.; Donini, O.; Cieplak, P.; Srinivasan, J.; Case, D. A.; Cheatham, T. E., III *Acc. Chem. Res.* **2000**, *33*, 889.

(44) Kollman, P. *Chem. Rev.* **1993**, *93*, 2395.

(45) Onufriev, A.; Bashford, D.; Case, D. A. *Proteins: Struct., Funct., Bioinf.* **2004**, *55*, 383.

(46) Hoel, P. G. In *Introduction to Mathematical Statistics*, 5th ed.; John Wiley & Sons: New York, 1984; pp 151−160.

(47) Prabu-Jeyabalan, M.; Nalivaika, E. A.; King, N. M.; Schiffer, C. A. *J. Virol.* **2003**, *77*, 1306.

(48) Prabu-Jeyabalan, M.; Nalivaika, E. A.; King, N. M.; Schiffer, C. A. *J. Virol.* **2004**, *78*, 12446.

(49) Tie, Y.; Boross, P. I.; Wang, Y. F.; Gaddis, L.; Liu, F.; Chen, X.; Tozser, J.; Harrison, R. W.; Weber, I. T. *FEBS J.* **2005**, *272*, 5265.
(50) Sugiura, W.; Matsuda, Zene.; Yokomaku, Y.; Hertogs, K.; Larder, B.; Oishi, T.; Okano, A.; Shiino, T,; Tatsumi, M.; Matsuda, M.; Abumi, H.; Takata, N.; Shirahata, S.; Yamada, K.; Yoshikura, H.; Nagai, Y. *Antimicrob. Agents Chemother.* **2002**, *46*, 708.
(51) Ode, H.; Ota, M.; Neya, S.; Hata, M.; Sugiura, W.; Hoshino, T. *J. Phys. Chem. B.* **2005**, *109*, 565.
(52) Ode, H.; Matsuyama, S.; Hata, M.; Neya, S.; Kakizawa, J.; Sugiura, W.; Hoshino, T. *J. Mol. Biol.* **2007**, *370*, 598.
(53) Ishima, R.; Ghirlando, R.; Tözsér, J.; Gronenborn, A. M.; Torchia, D. A.; Louis, J. M. *J. Biol. Chem.* **2001**, *276*, 49110.
(54) Louis, J. M.; Ishima, R.; Nesheiwat, I.; Pannell, L. K.; Lynch, S. M.; Torchia, D. A.; Gronenborn, A. M. *J. Biol. Chem.* **2003**, *278*, 6085.
(55) Coman, R. M.; Robbins, A. H.; Goodenow, M. M.; McKenna, R.; Dunn, B. M. *Acta Crystallogr.* **2007**, *F63*, 320.
(56) Coman, R. M.; Robbins, A. H.; Goodenow, M. M.; Dunn, B. M.; McKenna, R. *Acta Crystallogr.* **2008**, *D64*, 754.

JP908314F

Vaccine xxx (2009) xxx–xxx

Contents lists available at ScienceDirect

Vaccine

journal homepage: www.elsevier.com/locate/vaccine

T cell-based functional cDNA library screening identified SEC14-like 1a carboxy-terminal domain as a negative regulator of human immunodeficiency virus replication

Emiko Urano[a,b], Reiko Ichikawa[a], Yuko Morikawa[b], Takeshi Yoshida[c], Yoshio Koyanagi[c], Jun Komano[a,*]

[a] National Institute of Infectious Diseases, 1-23-1 Toyama, Shinjuku-ku, Tokyo 162-8640, Japan
[b] Graduate School of Infection Control Sciences, Kitasato University, Shirokane 5-9-1, Minato-ku, Tokyo 108-8641, Japan
[c] Laboratory of Viral Pathogenesis, Institute for Virus Research, Kyoto University, Kyoto 606-8507, Japan

ARTICLE INFO

Article history:
Received 16 May 2009
Received in revised form 7 July 2009
Accepted 24 July 2009
Available online xxx

Keywords:
HIV-1
SEC14L1a
Genome-wide screening

ABSTRACT

Genome-wide screening of host factors that regulate HIV-1 replication has been attempted using numerous experimental approaches. However, there has been limited success using T cell-based cDNA library screening to identify genes that regulate HIV-1 replication. We have established a genetic screening strategy using the human T cell line MT-4 and a replication-competent HIV-1. With this system, we identified the C-terminal domain (CTD) of SEC14-like 1a (SEC14L1a) as a novel inhibitor of HIV-1 replication. Our T cell-based cDNA screening system provides an alternative tool for identifying novel regulators of HIV-1 replication.

1. Introduction

The molecular interaction between HIV-1 and the host is not fully understood. A systematic genome-wide approach provides the critical information for the completion of the HIV-1-host interactome. Many experimental genome-wide screening systems have been established to identify the cellular genes required for HIV-1 replication (Table 1, [1–8]). More than a hundred genes have been identified as being cellular factors that regulate HIV-1 replication. However, different screening systems do not identify the same set of genes, and many systems yielded non-overlapping candidates. These discrepancies are assumed to be due to differences in the experimental approaches, such as the virus, the cell line, or the genetic materials used.

For viruses, the wild-type HIV-1 [1,3–6] or a replication-incompetent HIV-1 pseudotyped with vesicular stomatitis virus (VSV)-G is used [2,7,8]. The VSV-G-pseudotyped "HIV-1-based vector" has been used to identify factors associated with the viral entry processes. However, in reality, it covers the events from post-membrane fusion to translation. One of the potential caveats in the use of the VSV-G-pseudotyped vector is that it enters cells via the VSV-G-restricted route, which is fundamentally different from the HIV-1 *Env*-mediated entry pathway [9–12]. The replication-competent HIV-1 should be ideal to cover the entire viral replication cycle; however, this may raise biosafety concerns.

For cells, non-T cells, such as a genetically engineered HeLa cells that ectopically express luciferase or beta-galactosidase (TZM-bl cells), are often used, since they are efficiently transduced with genetic materials [2,5–8]. Not many studies employ a T cell-based system, partly because genetic materials are not efficiently transduced into T cells [1,3,4]. To identify HIV-1 replication regulatory factors, it is preferable to perform the functional analysis in the natural targets of HIV-1 including T cells. The gene expression profile of non-T cells is apparently different from that of T cells as exemplified by the absence of T cell specific markers on non-T cells such as CD4. It is possible that a candidate gene isolated in the non-T cell-based system might not be expressed in T cells. It is impossible to identify T cell-specific factors in the non-T cell-based screening using the siRNA library or in the screening using cDNA libraries derived from non-T cells. Also, the effect or functions of some genes may not be identical in distinct cell types. The potential risk of a non-T cell-based assay is that we may falsely score a gene as a regulator of HIV-1 replication, although many genes have been discovered using non-T cell-based screening systems including the viral receptors. Ideally, the primary CD4-positive T cells, dendritic cells, macrophages, or NK/T cells should be used.

* Corresponding author at: AIDS Research Center, National Institute of Infectious Diseases, 1-23-1 Toyama, Shinjuku, Tokyo 162-8640, Japan. Tel.: +81 3 5285 1111; fax: +81 3 5285 5037.
E-mail address: ajkomano@nih.go.jp (J. Komano).

0264-410X/$ – see front matter © 2009 Published by Elsevier Ltd.
doi:10.1016/j.vaccine.2009.07.084

Table 1
Summary of genome-wide screening strategies to identify regulatory factors of HIV-1 replication.

Genetic material	Transduction approach	Cell line	Replication competency of HIV-1	Reference
cDNA library	Retroviral, stable	TE671	Incompetent	[2,8]
siRNA library	Transfection, transient	HeLa or 293T	Competent or incompetent	[5,6,7]
cDNA library	Lenti- or retroviral, stable	MT-4	Competent	[1,3,4]

Given technical limitations, this is currently unrealistic for genetic screening experiments.

As for the genetic material, cDNA libraries are often used [1–4,8]. Recent studies utilized siRNA libraries [5–7]. The cDNA approach is advantageous for providing genetic diversity. Expression of the full-length open reading frame of a gene can upregulate the function of the gene, whereas cDNA fragments can function in a diverse fashion. The gene silencing approach downregulates gene expression; however, the silencing efficiency of a gene varies in different cell types and at different time points in the assay (reviewed in [13]). As mentioned above, the gene silencing approach is unable to score the contribution of genes that are not expressed in the cells used in the assay.

The screening can be performed in cells that are either transiently [5–7] or stably [1–4,8] transduced with genetic materials. In the transient transfection assays, it is possible that the dysregulation of a gene function can damage the physiology of the cells. In such a case, the inhibition of HIV-1 replication can be observed, but may not be a direct inhibitory effect of the gene of interest. Such a risk can be minimized by using cells stably transduced with the genetic materials.

We conducted a phenotype cDNA screen using a T cell line-based assay to identify cellular genes that render cells resistant to HIV-1 replication [3]. The advantage of our functional screening system is that cDNA libraries are stably transduced into cells, and that a replication-competent HIV-1 and a human T cell line MT-4 are used. With this system, we have successfully identified the SEC14-like 1a (SEC14L1a) C-terminal domain (CTD) as an inhibitor of HIV-1 replication that targets the late phase of the viral life cycle.

2. Materials and methods

2.1. Cells, transfection, cDNA selection

Cells were maintained in RPMI 1640 medium (Sigma, St. Louis, MA) supplemented with 10% fetal bovine serum (Japan Bioserum, Tokyo, Japan), 100 U/ml penicillin, and 100 μg/ml streptomycin (Invitrogen, Tokyo, Japan). Cells were incubated at 37 °C in a humidified 5% CO_2 atmosphere. Cells were transfected with Lipofectamine 2000 according to the manufacturer's protocol (Invitrogen). The method of selecting human cDNAs that confer resistance to HIV-1 has been described previously in detail [3].

2.2. Plasmids

The SEC14L1a CTD1 was amplified from MT-4 polyA RNA by reverse transcriptase PCR (RT-PCR) using the primers 5'-GCACCGGTCTCGAGCCACCATGGACTACAAAGACGATGACGACCCTGCGTGCGCCGCCAGCAGC-3′ and 5'-CCAATTGCTACCTGGAGATCATGGAGCTG-3'. The SEC14L1a CTD2 was amplified by PCR from human lymph node cDNA library (Takara, Otsu, Japan) using the primers 5'-GCACCGGTCTCGAGCCACCATGGACTACAAAGACGATGACGACTGCGAAGTGCCAGAGGGTGGAC-3' and 5'-CCAATTGCTACCTGGAGATCATGGAGCTG-3'. Full length (FL) SEC14L1a was amplified by PCR from a plasmid containing the SEC14L1a open reading frame (ORF, CS0DL004YN18, Invitrogen), using the primers 5'-GCACCGGTCTCGAGCCACCATGGACTACAAAGACGATGACGACGTGCAGAAATACCAGTCCCCAG-3' and 5'-CCAATTGCTACCTGGAGATCATGGAGCTG-3'. The AgeI-MfeI fragments of the PCR products were cloned into the XmaI-MfeI sites of the pEGFP-C3 plasmid (Clontech, Palo Alto, CA), generating pEGFP-SEC14L1a-CTD1, -CTD2, and -FL. The XhoI-MfeI fragments from the resulting plasmids were cloned into the corresponding restriction sites of the pCMMP KRAB vector, creating pCMMP GFP-SEC14L1a-CTD1, -CTD2, and -FL. The HIV-1 *tat* was amplified by PCR using the primers 5′-AACCGGTCTCGAGCCACCATGGAGCCAGTAGATCCTAGAC-3′ and 5′-GGATCCTCAGTCGTCATCGTCTTTGTAGTCTTCCTTCGGGCCTGTCGGGTC-3′. A Tat expression vector pCMMP Tat was constructed by cloning the AgeI-BamHI fragment of the PCR product into the corresponding restriction sites of the pCMMP KRAB vector. The HIV-1 *Env* and GFP expression vectors (pIIIex and pCMMP GFP, respectively) are described previously [3,12,14]. To construct the pCMMP GFP-FLAG (GFPf), pCMMP CXCR4 d-10 [15] was digested with AgeI and XhoI to remove CXCR4 d-10 ORF and self-ligated after blunting with T4 DNA polymerase. The HIV-1 *gag-pol*, *tat*, and *rev* expressing plasmid pCMVR8.91 was a generous gift from Dr. Trono's group [16].

2.3. Western blotting

Western blotting was performed according to techniques described previously [17]. The following reagents were used: anti-FLAG (rabbit polyconal, 600-401-383, Rockland, Gilbertsville, PA), anti-p24 (183-H12-5C, NIH AIDS Research and Reference Reagent Program), anti-gp120 (vA-20 and vT-21 antibodies, Santa Cruz Biotech, Santa Cruz, CA), biotinylated anti-goat antibody (GE Healthcare Bio-Sciences, Piscataway, NJ), horseradish peroxidase-conjugated streptoavidin (GE Healthcare Bio-Sciences), and EnVision+ system (Dako, Glostrup, Denmark). Signals were visualized with an LAS3000 imager (Fujifilm, Tokyo, Japan) and quantified by Multi Gauge ver 3.0 software (Fujifilm).

2.4. Confocal microscopy

293T cells transiently transfected with expression vectors for SEC14L1a derivatives were grown on glass plates, fixed in 4% formaldehyde in phosphate buffer saline (PBS) for 5 min at 24 h post-transfection, stained with Hoechst 33258 (Sigma), mounted (Vectorshield, Vector Laboratories, Burlingame, CA), and imaged using a confocal microscope META 510 (Carl Zeiss, Tokyo, Japan). For MT-4 cells, live cells were incubated with Hoechst 33258 and imaged unfixed. Image brightness and contrast were processed by META510 software (Carl Zeiss).

2.5. Immunoprecipitation

Cells expressing FLAG-tagged proteins were harvested and washed twice with PBS and then lysed in the lysis buffer (50 mM Tris–HCl, pH 8.0, 0.5% IGEPAL CA630, protease inhibitor cocktail from Sigma) on ice for 30 min. The soluble fraction was obtained by centrifugation at 15,000 rpm for 30 min at 4 °C, and was incubated with 20 μl of Red-Anti-FLAG M2 Affinity Gel (Sigma) with gentle mixing overnight at 4 °C. After washing the agarose beads for five times with the lysis buffer, the bound complexes were eluted with the FLAG peptide, and analyzed by Western blotting.

Please cite this article in press as: Urano E, et al. T cell-based functional cDNA library screening identified SEC14-like 1a carboxy-terminal domain as a negative regulator of human immunodeficiency virus replication. Vaccine (2009), doi:10.1016/j.vaccine.2009.07.084

2.6. Flow cytometry

Cells were labeled with PE-Cy5-conjugated anti-CD4 antibody or PE-conjugated anti-CXCR4 antibody (Beckton Dickinson, San Jose, Calif.) for 30 min at 4 °C. Cells were washed once with PBS supplemented with 1% FBS and analyzed by FACS Aria (Beckton Dickinson). The GFP-positive cells were sorted using FACS Aria.

2.7. Monitoring HIV-1 replication

For HIV-1 infection, 1×10^5 cells were incubated at the room temperature with the HIV-1_{HXB2}-containing culture supernatant, which had approximately 1.0 ng of $p24^{CA}$, for approximately 30 min. The culture supernatants were collected at 4 d post-infection and subjected to ELISA to measure the $p24^{CA}$ antigen, using a Retro TEK p24 Antigen ELISA Kit according to the manufacturer's protocol (Zepto Metrix, Buffalo, NY). The signals were measured with an ELx808 microplate photometer (BIO-TEK®, Winooski, VT).

2.8. PCR analysis

The cellular DNA and RNA were extracted from cells infected with VSV-G-pseudotyped HIV-1 vector produced by using pNL-Luc plasmid, as described previously [17]. The Alu-LTR PCR and RT-PCR were performed as described previously [3,17] using the following primers: for the first Alu-LTR PCR reaction, 5'-AACTAGGGAACCCACTGCTTAAG-3' and 5'-TGCTGGGATTACAGGC-GTGAG-3'; and for the second Alu-LTR PCR reaction, 5'-AACT-AGGGAACCCACTGCTTAAG-3' and 5'-CTGCTAGAGATTTTCCACA-CTGAC-3'. For amplification of HIV-1 mRNA, 5′-ATGGAGCCAGTAG-ATCCTAGAC-3′ and 5′-CTATTCCTTCGGGCCTGTCGGG-3′ primers were used. For the control, we amplified beta-globin and cyclophilin A using the following primers: beta-globin, 5'-TATTGGTCT-CCTTAAACCTGTCTTG-3' and 5'-CTGACACAACTGTGTTCACTAGC-3'; and cyclophilin A, 5′- CACCGCCACCATGGTCAACCCCACCGTGTTCT-TCGAC-3′ and 5′- CCCGGGCCTCGAGCTTTCGAGTTGTCCACAGTCA-GCAATGG-3′. The amplicons were separated in a 2% agarose gel, stained with ethidium bromide, and imaged with a Typhoon scanner (GE Healthcare Bio-Sciences).

2.9. Collection of virus-like particle

Tissue culture supernatants containing virus-like particles (VLP) were passed through nitrocellulose filters (0.45 μm, Millipore, Tokyo, Japan) and the virions were collected by centrifugation (Optima™ TL, TLA 100.3 rotor, 541 k × g for 1 h; Beckman Coulter, Miami, FL).

3. Results

3.1. Identification of SEC14L1a as a potential regulator of HIV-1 replication

We prepared MT-4 cells that constitutively express cDNA transduced by a lentiviral vector or an MLV-based retroviral vector (Fig. 1A). The cDNAs were derived from human peripheral blood mononuclear cells (PBL) and *Oryctolagus cuniculus* (European rabbit) kidney-derived cell line RK13 cells. MT-4 cells transduced with cDNA were collected by FACS sorter using the green fluorescence as a marker since viral vectors encoded the GFP expression cassette. Then, cells were infected with HIV-1. Surviving cells were propagated and the genomic DNA was extracted to recover the transduced cDNA by PCR as previously described [3]. We isolated two clones encoding the carboxy terminal domain (CTD) of SEC14L1a (Gene ID 6397, Fig. 1B and C); one from the PBL cDNA library (1/65 independent clones, 1.5%), and one from the RK13 cDNA library (1/42 independent clones, 2.4%). The fact that the SEC14L1a CTD was successfully identified from two independent cDNA libraries strongly suggests that it is a negative regulator of HIV-1 replication. It is important to note that previous genome-wide screenings for HIV-1 regulators have not identified SEC14L1a CTD. This clearly suggests that our T cell-based cDNA screening system is unique, and should be able to complement the other genome-wide screening systems.

SEC14L1a belongs to the widely-expressed SEC14-superfamily that is involved in membrane trafficking and phospholipid metabolism [18–21]. The function of SEC14L1a is not well understood. The C-terminus of SEC14L1a encodes a Golgi dynamics (GOLD) domain (amino acids (aa) 523–674; Fig. 1C) that mediates the protein-protein interaction possibly involved in the maintenance of Golgi apparatus function and vesicular trafficking [22]. The only reported biological activity of SEC14L1a is to interact with cholinergic receptors AchT and CHT1 [23]. The GOLD domain is responsible for the physical interaction between SEC14L1a and cholinergic receptors. However, the functional significance of these interactions remains to be clarified. The conserved SEC14 domain directly interacts with lipid molecules [17–21]. However, the lipid ligand of SEC14L1a (aa 319–490, Fig. 1C) has yet to be identified.

3.2. Construction of expression vectors for SEC14L1a derivatives

The longest SEC14L1a cDNA recovered from the PBL cDNA library spanned nucleotides (nt) 2045–2492 of SEC14L1a mRNA (NM_003003.3), covering the CTD of the SEC14L1a open reading frame (ORF; Fig. 1B). We detected a potential translational start codon at nt 2188-2190 within the GOLD domain (asterisk, Fig. 1B). We speculated that the isolated cDNA might have expressed the carboxy half of the GOLD domain (aa 641–715) in MT-4 cells, leading to the inhibition of HIV-1 replication.

To test this, we constructed an expression plasmid for FLAG-tagged CTD (aa 642-715) fused to the carboxy terminus of GFP (CTD1; Fig. 1C). We also constructed GFP fusion proteins spanning the GOLD domain (CTD2, aa 493–715) or the full-length SEC14L1a (FL; Fig. 1C). Expression of these proteins was verified by Western blotting of transient transfected 293T cells (Fig. 1D). The confocal microscopy analysis indicated that the FL localized mainly in the cytoplasm, with some accumulation in the perinuclear regions (Fig. 1E), consistent with a previous report [23]. CTD1 was distributed in the cytoplasm and the nucleus, with a slight preference for the cytoplasm. CTD2 was evenly distributed to the nucleus and cytoplasm. When MT-4 cells constitutively expressing FL, CTD1, and CTD2 were analyzed, the subcellular distribution was less clear, due to the small cytoplasm (Fig. 1F). However, FL was distributed evenly to the nucleus and cytoplasm in MT-4 cells. In contrast, CTD1 was excluded from the nucleus in MT-4 cells (Fig. 1F). The distribution of CTD2 in MT-4 cells was similar to that in 293T cells (Fig. 1F). The differences of protein distribution in two cell types may be caused by the cell type-dependent regulation of protein trafficking and/or the effect of protein expression levels.

3.3. Verification of anti-HIV-1 activity associated with SEC14L1a CTD1

We introduced FL, CTD1, or CTD2 into MT-4 cells using the MLV vector, and isolated cells constitutively expressing FL, CTD1, or CTD2. Expression of SEC14L1a derivatives in MT-4 cells was verified by Western blotting (Fig. 2A). FL expression was verified by immuno-precipitation assay (Fig. 2A). The detection of FL by Western blotting was inefficient considering the fact that all the SEC14L1a derivatives are GFP-tagged, and the GFP intensity of FL-expressing MT-4 cells was not lower than that of CTD1-expressing

Please cite this article in press as: Urano E, et al. T cell-based functional cDNA library screening identified SEC14-like 1a carboxy-terminal domain as a negative regulator of human immunodeficiency virus replication. Vaccine (2009), doi:10.1016/j.vaccine.2009.07.084

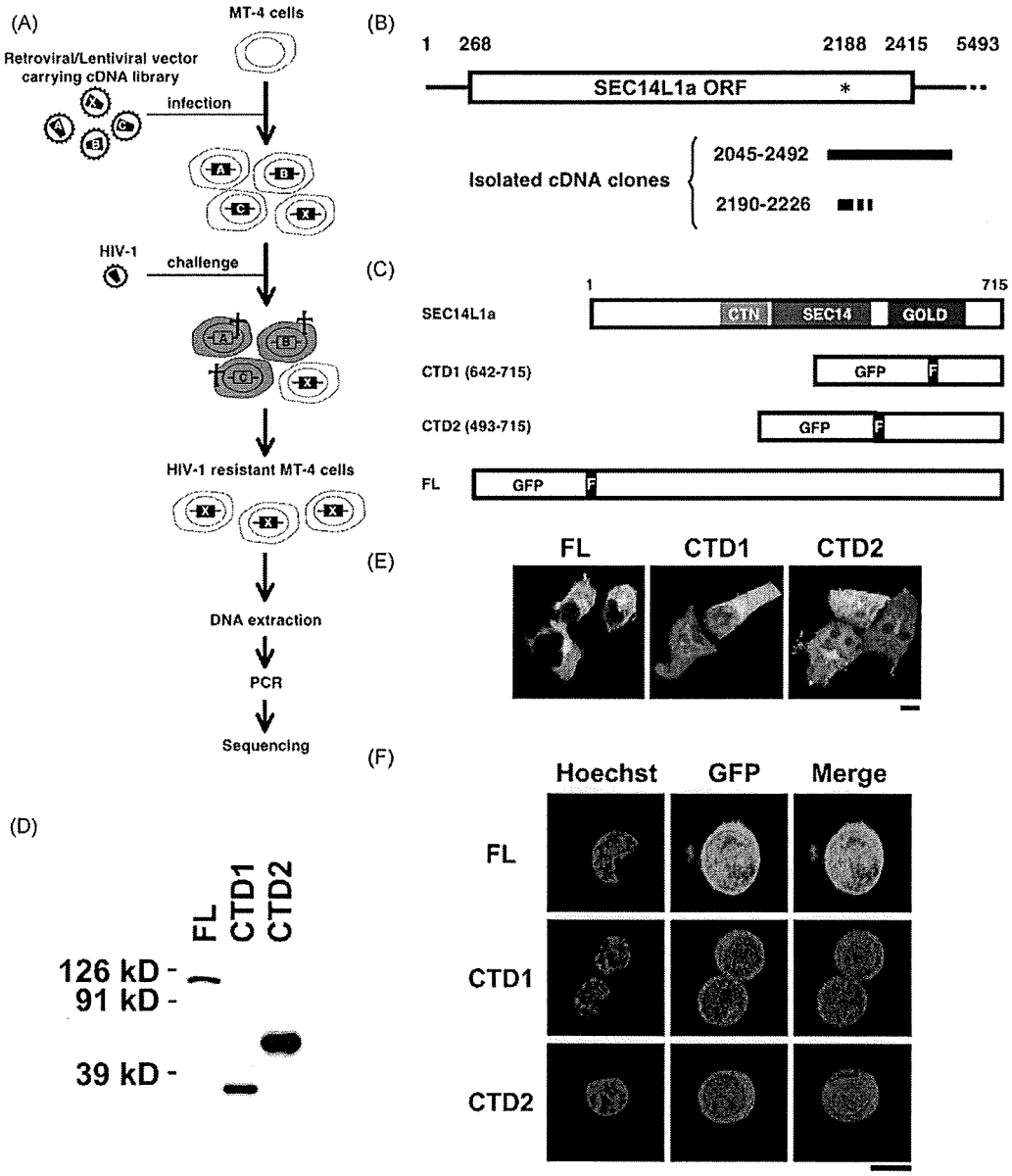

Fig. 1. Identification of SEC14L1a CTD as a potential regulator of HIV-1 replication. (A) The experimental strategy used to screen a cDNA library for genes rendering cells resistant to HIV-1. MT-4 cells were infected with a retroviral or lentiviral vector carrying cDNA libraries and were challenged with wild-type HIV-1_{HXB2}. The HIV-1-infected cells (gray with cross) quickly undergo cell death. The surviving cells were propagated, collected, and the transduced cDNA labeled X was determined. (B) Schematic representation of SEC14L1a mRNA (NM_00303.3) and the isolated gene fragments. The open reading frame (ORF) is assigned from nucleotides (nt) 268 to 2415. The potential internal translational initiation codon is marked with an asterisk. (C) Schematic representation of the SEC14L1a protein (NP_002994). SEC14L1a has a CRAL_TRIO_N domain (CTN, amino acids 241–313), a SEC14p-like lipid-binding domain (SEC14, amino acids 319–490), and a Golgi dynamics domain (GOLD, amino acids 523–674). The cloned fragments (CTD1 and CTD2) and full-length (FL) gene were tagged with a FLAG epitope (indicated with an "F") on their N-termini, and fused to the C-terminus of GFP. (D) Verification of FL, CTD1, and CTD2 expression in 293T cells by Western blotting using anti-FLAG antibody. (E) Confocal microscopy images of 293T cells expressing FL, CTD1, or CTD2. The green signal represents GFP fluorescence. Magnification, 630×; scale bar, 10 μm. (F) Confocal microscopy images of MT-4 cells constitutively expressing FL, CTD1, or CTD2. The blue signal represents the Hoechst-stained nucleus, and green represents GFP fluorescence. Magnification, 630×; scale bar, 5 μm.

cells (Fig. 1F). The MLV vector expressing GFP alone was used as a control. The cell proliferation, morphology, and cell surface levels of HIV-1 receptors were unaltered by any of the SEC14L1a derivatives (Fig. 1F, 2B, and data not shown). HIV-1 replication was tested in these cells. The level of HIV-1 replication was significantly inhibited in CTD1- and CTD2-expressing cells (69.1% and 69.8% on the average from seven independent experiments, respectively, $P < 0.05$, two-tailed Student's t-test), but was hardly inhibited in FL-expressing cells (86.4%, not statistically significant; Fig. 2C). This observation was reproducible in independently established MT-4 cells and SupT1 cells (data not shown). These data verified the original screening results, and suggest that the C-terminal half of GOLD domain of SEC14L1a serves as an inhibitor of HIV-1 replication. In contrast, it is suggested that FL is not a potent negative regulator of HIV-1 replication.

3.4. SEC14L1a CTD1 and CTD2 target the late phase of the HIV-1 life cycle

We analyzed the viral entry and production phases to determine which step of the HIV-1 life cycle CTD1 and CTD2 target.

The Alu-LTR PCR assay was performed to examine the effect of SEC14L1a derivatives on the viral entry phase. The MT-4 cells stably expressing GFP, FL, CTD1, or CTD2 were infected with VSV-

Please cite this article in press as: Urano E, et al. T cell-based functional cDNA library screening identified SEC14-like 1a carboxy-terminal domain as a negative regulator of human immunodeficiency virus replication. Vaccine (2009), doi:10.1016/j.vaccine.2009.07.084

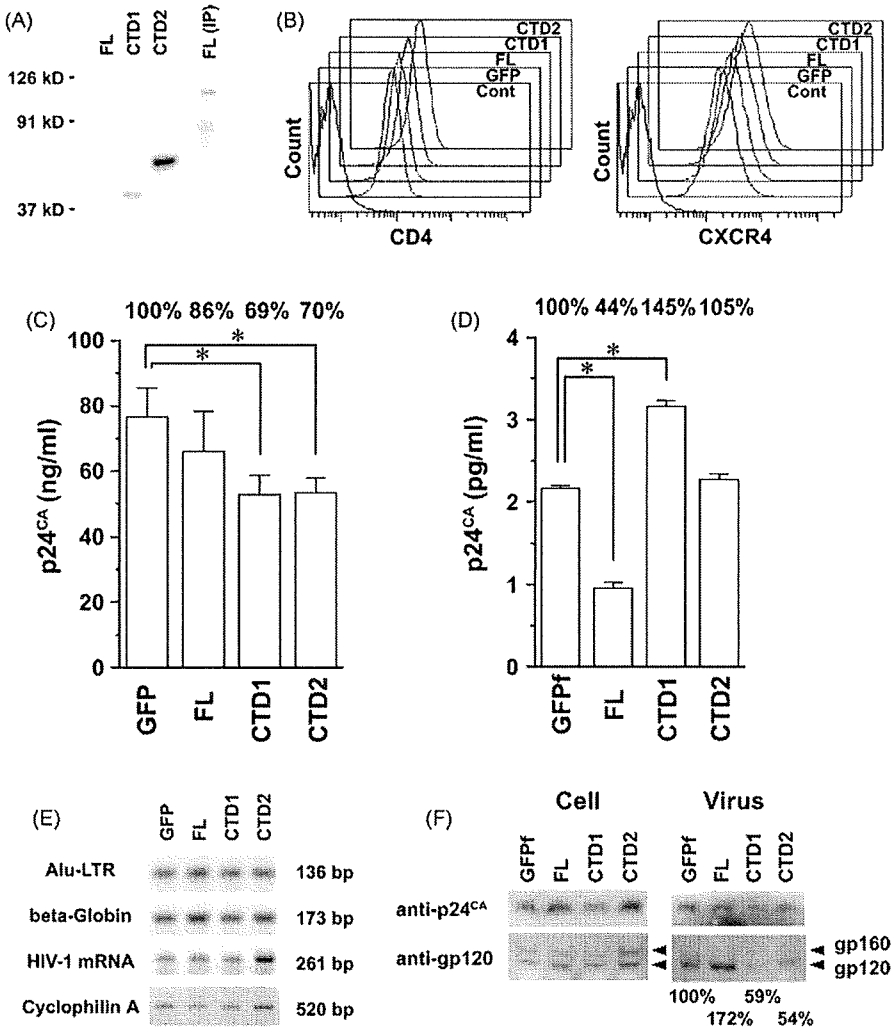

Fig. 2. Functional characterization of the SEC14L1a derivatives. (A) Detection of stable expression of FL, CTD1, and CTD2 in MT-4 cells by Western blotting using anti-FLAG antibody. FL was detected by the immunoprecipitation (IP) assay using agarose beads conjugated with anti-FLAG antibody. The flow cytometric analysis of the cell surface expression of HIV-1 receptors CD4 and CXCR4 in MT-4 cells stably expressing GFP, FL, CTD1, and CTD2. (C) Constitutive expression of CTD1 and CTD2 limited the replication of HIV-1 in MT-4 cells. The concentration of viral $p24^{CA}$ antigen in the culture supernatant was measured at 4 d post-infection. The results represent the average of seven independent experiments ± the standard error of the mean. The reduction of viral $p24^{CA}$ concentration relative to GFP was shown on the top. Asterisks indicate the statistical significance compared to GFP ($P < 0.05$ by two-tailed Student's *t*-test). (D) The PCR-based assay to examine the effect of SEC14L1a derivatives on the early phase of viral life cycle (top two panels) and the transcription from LTR promoter (bottom two panels). The HIV-1 entry efficiency was examined by Alu-LTR PCR. Beta globin was used as an internal control. The HIV-1 transcription efficiency was examined by RT-PCR targeting spliced viral mRNA. Cyclophilin A was used as a control. The expected length of each PCR amplicon was indicated. (E) The effect of SEC14L1a derivatives on the HIV-1 production. The 293T cells grown in a well of a 6-well plate were transfected with 200 ng of HIV-1 proviral DNA and 2 μg of expression vector for GFPf, FL, CTD1, or CTD2. The culture supernatant was recovered at 2 d post-transfection and the $p24^{CA}$ concentration was measured. The representative data from five independent experiments was shown. The results indicate the average ± the standard deviation. The relative $p24^{CA}$ concentration compared to GFPf was shown on the top. Asterisks indicate the statistical significance compared to GFPf ($P < 0.001$ by two-tailed Student's *t*-test). The *Env* incorporation onto the virus-like particles (VLP) produced by 293T cells expressing SEC14L1a derivatives. The 293T cells grown in a well of a 6-well plate were transfected with 1 μg of *gag-pol* (pCMVR8.91) and *Env* (pIIIex) expression vectors along with 2 μg of expression vector for GFPf, FL, CTD1, or CTD2. The cell lysates (Cell) and VLP fractions (Virus) were subjected to Western blot analysis detecting gp120 and $p24^{CA}$ harvested at 2 d post-transfection. The *Env* incorporation levels normalized to $p24^{CA}$ relative to GFPf were shown at the bottom.

G-pseudotyped HIV-1 vector, and the cellular genomic DNA was recovered at 4 d post-infection. The amount of Alu-LTR PCR products from FL-, CTD1-, or CTD2-expressing MT-4 cells was almost equal to that from GFP-expressing cells, suggesting that the early phase of the viral life cycle is not inhibited by any of the SEC14L1a derivatives (Fig. 2D). To examine the viral production phase, we examined the LTR-driven viral gene transcription by RT-PCR. Cellular RNA was extracted from the same MT-4 cells infected with VSV-G-pseudotyped HIV-1 vector, and RT-PCR was conducted to amplify LTR promoter-driven spliced HIV-1 mRNA. The amount of viral RNA expressed in FL-, CTD1-, or CTD2-expressing cells was not lower than that in GFP-expressing cells when the levels of the internal control was taken into account (Fig. 2D). Given that the similar number of viral genome was integrated as indicated by the Alu-LTR PCR, these data suggest that viral transcription is not inhibited by any of the SEC14L1a derivatives, and that the action point of CTD1 and CTD2 should be at post-transcriptional levels of the viral production phase.

Next, the FL, CTD1, or CTD2 expression vector was co-transfected with HIV-1 proviral DNA into 293T cells, and viral production was quantified by $p24^{CA}$ ELISA. The FLAG-tagged GFP (GFPf) was used as a control hereafter. We found that the FL expression significantly reduced the production of HIV-1 (44.2%, $P < 0.001$, two-tailed Student's *t*-test) compared to the GFPf control (Fig. 2E). In contrast, the CTD1 enhanced the production of HIV-1 (145.9%, $P < 0.001$, two-tailed Student's *t*-test; Fig. 2E). However, CTD2 did not measurably affect the HIV-1 production (105.1%, not statistically significant; Fig. 2E). As the ELISA assay examines the effect

Please cite this article in press as: Urano E, et al. T cell-based functional cDNA library screening identified SEC14-like 1a carboxy-terminal domain as a negative regulator of human immunodeficiency virus replication. Vaccine (2009), doi:10.1016/j.vaccine.2009.07.084